First-principles calculations of the three-dimensional structure and intrinsic defects in *trans*-polyacetylene

P. Vogl* and D. K. Campbell
Center for Nonlinear Studies, Los Alamos National Laboratory, Los Alamos, New Mexico 87545
(Received 22 November 1989)

We report a first-principles, local-density-functional (LDA) calculation of the electronic structure of crystalline, three-dimensional (3D) *trans*-$(CH)_x$. For the perfect crystal, we find a broken-symmetry ground state having $P2_1/a$ space-group symmetry, corresponding to *in*-phase dimerization on neighboring chains within the unit cell. We show that in this structure the interchain couplings, although weak, lead to an asymmetry between the valence and conduction bands and, more importantly, give 3D character to the electronic band-edge states. We investigate several additional aspects of the electronic structure of the perfect crystal, including self-consistent optimization of the ions in the unit cell, spin polarization and electronic charge densities, interchain electron-phonon interactions, and the density of states. To study intrinsic defects in *trans*-$(CH)_x$, we map our LDA results onto a multi-orbital, tight-binding model; this mapping preserves very accurately all the electronic-structure properties of the full calculation. Using a Koster-Slater Green-function technique, we are able to examine both (shallow) polaronlike and (deep) bipolaronlike lattice distortions corresponding to localized defects. We find that the 3D character of the electronic band-edge states strongly suppresses the formation of the self-trapped, localized defects characteristic of the 1D models, destabilizing polarons and possibly bipolarons as well in perfectly ordered 3D *trans*-$(CH)_x$. To establish a connection with earlier work, we demonstrate that by artificially decreasing interchain effects and/or increasing the intrachain electron-phonon coupling we can cause polarons and bipolarons to form. We examine the agreement of our results for the idealized perfectly crystalline material with experimental results on real samples of *trans*-$(CH)_x$ and conclude with suggestions for future work, both theoretical and experimental.

I. INTRODUCTION

Our goal in this article is to calculate, and to develop a qualitative understanding of, the electronic structure and the intrinsic defects of three-dimensional, crystalline *trans*-polyacetylene [*trans*-$(CH)_x$]. To motivate our study, and to clarify its context as well, we begin by recalling several aspects of the long-standing debate on the microscopic modeling of conducting polymers and the corresponding finite oligomers.

Most of this continuing debate has focused on the relative importance of electron-electron (e-e) versus electron-phonon (e-p) interactions (for reviews, see Refs. 1–6). The two major current schools of thought on this issue can usefully (although not entirely accurately) be characterized as the "chemical" and "physical" schools. To chemists, *trans*-$(CH)_x$ is simply the "infinite" polyene. The extensive chemical literature on *finite* polyenes, which dates back at least as far as Hückel[7] (see also Salem[8]), initially dealt primarily with the question of bond alternation and thus concentrated on the coupling between the π electrons and the nuclear coordinates (or, in modern parlance, on the e-p interactions). More recently, the irrefutable evidence[9] that single-particle theories—be they pure e-p or Hartree-Fock, incorporating e-e interactions in the mean-field approximation—cannot capture the observed ordering of excited states[9,10] in finite polyenes has led the "chemical school" to focus chiefly on models for $(CH)_x$ in which the e-e interactions play the dominant role. These models have achieved considerable success; for example, exact diagonalizations of the Pariser-Parr-Pople[11] model for finite oligomers involving up to 12 (CH) units[12,13] (dodecahexaene) have produced results consistent both with experiments on finite polyene excited states[9] and with ENDOR measurements[14,15] of spin densities in polyacetylene.

To physicists, on the other hand, the successes of single-electron approaches in metals or semiconductors strongly suggest that in the conducting polymers "solid-state effects" conspire to reduce the importance of the atomic or molecular Coulomb forces that exist in the isolated, finite oligomers. Thus, although there have been attempts within the physics literature to explain the optical gap in *trans*-$(CH)_x$ using (the Mott-Hubbard model of) e-e interactions,[16] conventional wisdom in physics has favored a single-electron approach emphasizing e-p interactions. The celebrated Su-Schrieffer-Heeger (SSH) model,[17] for example, explains both the bond alternation[18,19] and the optical gap observed in *trans*-$(CH)_x$ entirely in terms of e-p interactions and the resulting Peierls instability in one-dimensional systems. Further, the SSH model predicts a variety of localized, nonlinear excitations—kink solitons, polarons, and [in *cis*-$(CH)_x$ and similar polymers] bipolarons—with theoretically well-characterized effects on magnetic and optical properties. These theoretical predictions have stimulated, and

been generally consistent with, a large body of experimental work.[1,3]

One obvious way to reconcile the distinct perspectives of the "chemical" and "physical" schools is to treat one-dimensional models in which both (*e-e*) and (*e-p*) interactions are incorporated; considerable effort has recently been devoted to this approach (for reviews, see Refs. 1, 3, and 5). A second way to reconcile the two perspectives is to take seriously the idea that "solid-state effects"—e.g., screening due to adjacent chains, effects due to crystalline order—may make the conducting polymers quite different from the isolated finite polyenes. Clearly, to study these solid-state effects realistically, one must have an accurate model of the actual three-dimensional solid material; this requirement immediately provides one motivation for our calculation.

Surprisingly, in contrast to the very extensive effort devoted to the studies of strictly one-dimensional (1D) models, substantially less attention has been paid to the effects that arise because the real samples of *trans*-$(CH)_x$, although microscopically highly anisotropic, are in fact inherently *three*-dimensional (for reviews see Refs. 20 and 21). In addition to the possibility that the interchain couplings that arise in the solid material may lead to substantial differences between the current forms of *trans*-$(CH)_x$ and the finite polyenes in gas phase or solution and thus may rationalize the differences in expectations based on the chemists' and physicists' approaches, theoretical studies[22,23] have suggested that the interchain couplings can affect strongly the nature and properties of the novel nonlinear excitations predicted on the basis of the strictly 1D theories. This greatly increases the interest both in an accurate calculation of the three-dimensional (3D) structure of *trans*-$(CH)_x$ and in the development of a qualitative understanding of this structure and thus provides an additional motivation for our study.

Before describing our approach in detail, it is important to place our work in the context of earlier investigations of the effects of dimensionality in conducting polymers. Among the pioneering works that calculated the 3D structure of polyacetylene in both the *cis*- and *trans*-$(CH)_x$ isomers were studies employing chemical approaches based on packing and bonding arguments[24–27] and investigations using physical approaches based on band theory and variants of local-density-functional theory.[28–32] These studies confirmed the expected anisotropy of the material and, in some cases, provided detailed insight into the 3D band structure. However, they did not address the issue of theoretical expectation for the ground state of crystalline *trans*-$(CH)_x$. To phrase the issue in terms of a specific question (using terminology that will be defined precisely in later sections), is the ground state of *trans*-$(CH)_x$ predicted to have $P2_1/n$ symmetry (as deduced from early experiments on polycrystalline films of the Shirakawa material[18]) or $P2_1/a$ symmetry [as deduced from more recent experiments[33,34] on highly-oriented films of "Durham" *trans*-$(CH)_x$]? Perhaps more importantly, although numerous studies[23,35–40] based on simplified models have suggested that 3D interchain coupling can have dramatic effects on the nonlinear excitations predicted by the 1D theories, previous *ab initio* calculations[28–32,41–45] of the 3D structure of both *trans*-- and *cis*-$(CH)_x$ have left for further investigations the critical question of whether the interchain couplings are sufficiently strong to destabilize the carrier self-trapping associated with intrinsic defects in 1D systems. In addition, the more general issue of the relation of the 3D predictions to the more familiar 1D results seems insufficiently explored. These issues provide still further motivation for our investigations.

Accordingly, in the present article we continue an extensive new first-principles study—initiated in two previous short communications[46,47]—of the 3D structure of *trans*-$(CH)_x$. Our approach is based on Hohenberg-Kohn-Sham density-functional theory treated in both the local-density approximation (LDA) and the local-spin-density approximation (LSDA). We attempt to develop a unified picture of *trans*-$(CH)_x$ by relating our results to those of previous studies in both one and three dimensions.

At the outset, we should underscore the difficulties that the materials aspects of real samples of *trans*-$(CH)_x$ pose for any attempts to extract "intrinsic" properties of the pure, "crystalline" material. If prepared by the Shirakawa method, using a Ziegler-Natta chemical catalyst, *trans*-$(CH)_x$ films have less than full density (≈ 0.4 g/cm^3) and on a microscopic scale (200–1000 Å) consist of tangled fibrils which, by stretching, can be partially aligned. Changes in the catalysis conditions can lead to substantial differences in the mesoscale morphology (for a discussion and additional references see Ref. 48). The degree of microscopic crystallinity in the standard Shirakawa material is thought to be as high as 75–90 % but the disordered regions are not well understood.[21] Further, Shirakawa *trans*-$(CH)_x$ contains $\approx 10^{19}$/cm^3 "free spins",[49] often interpreted as neutral solitons or as dangling bonds and/or radicals, as well as charged "impurity" states,[50] thought to be related to inadvertent doping by the Ziegler-Natta catalyst, at the level of $\approx 10^{18}$/cm^3. If prepared by the so-called "Durham" route, using a processible prepolymer and thermal elimination, *trans*-$(CH)_x$ can be made into fully dense (≈ 1.2 g/cm^3) films that are mesoscopically fairly uniform. The films can be made in either an "oriented" form—made by stretching the prepolymer—or a "nonoriented" form. The former is observed to be more crystalline and appears to have average conjugation lengths on the order of $n = 30$–40, whereas the latter seem to be amorphous and has an average conjugation length of $n = 11$–14.[51] The levels of intrinsic defects and impurity contamination are not yet fully characterized. Various attempts to produce isolated chains in the solid state using either matrices or copolymer techniques add still greater variety (more accurately, confusion) to the picture. In our LDA calculation, we shall focus almost entirely on pristine, crystalline *trans*-$(CH)_x$. If, as one might expect, the interchain interactions are substantially modified by a lack of crystalline order, some of our conclusions may not *a priori* apply to the currently available materials.

In Sec. II A we discuss the methodology of our LDA and LSDA calculations, comparing and contrasting them with earlier structure calculations based on both chemi-

cal methods[24–27] and on LDA approaches in both 1D variants[43–45,52] and 3D variants.[28–30,32,42,53] In Sec. II B we review the nomenclature and methodology for characterizing the 3D structure of *trans*-$(CH)_x$. In particular, we recall that whereas the initial x-ray studies[18] on Shirakawa *trans*-$(CH)_x$ suggested a $P2_1/n$ structure, more recent investigations of Durham $(CH)_x$, using both electron microscopy[53] and x-ray diffraction,[34] suggest a $P2_1/a$ structure. However, the two sets of structural data agree within errors on the lattice parameters.

Section II C contains the results of our study of crystalline *trans*-$(CH)_x$. Taking the experimentally observed lattice constants a, b, and c and the monoclinic angle β as given, we show that the LDA results favor the $P2_1/a$ structure over the $P2_1/n$, by an amount which (given the similarities of the two structures) is calculationally significant; we then suggest a qualitative physical interpretation of this result. Nonetheless, in view of the remaining uncertainties, and for comparison to previous results, both here and in later sections we study the $P2_1/n$ structure in some detail. We next present a series of studies of specific aspects of the structural and electronic properties of the fully 3D material, including the optimized position of the ions in the unit cell, the spin polarization and electronic charge densities, the band structure, the interchain electron-phonon interaction, and the density of states.

In Sec. III we turn to the issue of intrinsic defects in *trans*-$(CH)_x$. To make the calculations tractable, we develop a 3D, multi-orbital tight-binding model which reproduces very accurately the LDA structural and electronic properties found in Sec. II C. Within this model, we use the Koster-Slater Green-function approach[54] to examine localized defects in the otherwise perfect crystal. We study intrinsic defects including kink solitons, polarons, and bipolarons, in which both lattice deformations and electronic structure play a role. As expected, the interchain interactions preclude the formation of free, unbound kink solitons;[22] instead, only bound kink-antikink pairs—in essence, polarons or bipolarons—can be formed. Significantly, a calculation of the electronic structure corresponding to a localized (shallow) polaron-like defect shows that for reasonable ranges of the lattice distortion there are no states in the gap and hence no localized electronic states. To establish consistency with earlier work, we demonstrate that, by artificially decreasing interchain effects and/or increasing the electron-phonon coupling, we can cause the polaron to form. For deep bipolaron distortions, we also find that the intragap levels arise only for fairly large values of the lattice distortion, again because of 3D effects. Thus, our results suggest that interchain coupling effects are likely to destabilize the 1D polaron and possibly also the bipolaron in crystalline *trans*-$(CH)_x$.[23]

In Sec. V we present a discussion of our findings and our conclusions. We examine the limitations of our results, mentioning in particular the difficulties that "strongly correlated" systems pose for the LDA approach. We also examine the consistency of our findings for ideal, pristine *trans*-$(CH)_x$ with experimental results, including optical absorption, on real samples. We conclude with suggestions for future work, both theoretical and experimental.

II. STRUCTURAL AND ELECTRONIC PROPERTIES OF CRYSTALLINE *trans*-$(CH)_x$

A. Description of the local-density approach to *trans*-$(CH)_x$

To calculate the ground-state properties of crystalline *trans*-$(CH)_x$, we have employed local-density-functional theory both in spin-polarized and spin-unpolarized forms,[55] using the *ab initio* pseudopotential plane-wave method.[56,57] Local-density-functional theory has been shown to reproduce accurately the structural properties of a broad range of atoms,[58,59] molecules,[60] and solid-state systems,[61,62] including semiconductors, insulators, and even van der Waals crystals[63] from first principles. In most cases, quantities involving the total energy, such as lattice constants, bulk moduli, phonon frequencies, charge densities, and structural stabilities, have been found to agree within a few percent of experimental values.

The method has two major weaknesses which are relevant for polyacetylene. First, local-density-functional theory, being rigorously applicable only to the ground state, is notorious for underestimating the energy gap in semiconducting phases. The essential source of the discrepancy is not the local-density approximation (LDA) but the neglect of a discontinuity in the exact exchange-correlation potential across the gap.[64] Fortunately, calculations of the electron self-energies for a range of materials have revealed that the "true" quasiparticle bands differ from the LDA bands predominantly by a rigid upward shift, $\Sigma_{\rm con}$, of the conduction bands that is weakly dependent on the electron momentum.[65–67] Second, the local-density approach accounts only semiquantitatively for phase transitions which are driven by strong electron correlations, even when the spin-polarized version of local density theory (LSDA) is employed. Thus, the theory correctly predicts the antiferromagnetic ground state of MnO and of the half-filled Hubbard model, for example, but it underestimates the correlation gap and fails altogether when f, the fractional band filling, does not equal 0.5.[68,69] On the other hand, structural phase transformations which are driven by strong electron-phonon interactions, such as ferroelectric transitions,[70] or pressure-induced phase transitions in solid hydrogen halides,[71] are accurately accounted for by the LDA.

In the present work, the total energy of *trans*-$(CH)_x$ is calculated within local-density-functional theory using the formalism of Ihm *etal.*[57] in the plane-wave representation. In this approach, the total energy is expressed as a sum of terms,

$$E_{\rm tot}=E_{\rm tot,el}+E_{\rm core\text{-}core}\ , \tag{2.1}$$

$$E_{\rm tot,el}=E_{\rm kin}+E_{\rm el\text{-}core}+E_{\rm el\text{-}el}\ , \tag{2.2}$$

where $E_{\rm kin}$ is the kinetic energy of the electrons, $E_{\rm core\text{-}core}$ is the Coulomb interaction between the ion cores, $E_{\rm el\text{-}core}$ is the electron-core interaction, and $E_{\rm el\text{-}el}$ is the electron-electron interaction. The electron-ion interaction $E_{\rm el\text{-}core}$ is determined using the Coulomb potential for hydrogen

and norm-conserving *ab initio* carbon pseudopotentials generated in Ref. 72. We note that carbon, with its small core consisting only of the 1*s* state, is a good candidate for the *ab initio* pseudopotential approach, because the core wave functions do not overlap significantly with the valence functions, and the core eigenvalues are well separated from the valence eigenvalues.

The electron-electron interaction consists of the Hartree energy and the exchange-correlation energy, which is evaluated with the accurate local-density functional given by Painter for the spin-unpolarized and the spin-polarized cases.[73] This functional is based on Monte Carlo calculations of the correlation energy in the electron gas.[74]

The electronic energy, Eq. (2.2), is determined by solving self-consistently the Kohn-Sham equations, which in their spin-polarized form[75,76] read

$$\left[-\frac{\hbar^2}{2m_e}\nabla^2+V_{\rm ion}(\mathbf{r})+V_H(\mathbf{r})+\mu_{{\rm xc},\sigma}(\mathbf{r})\right]\psi_{i,\sigma}(\mathbf{r}) =\varepsilon_{i,\sigma}\psi_{i,\sigma}(\mathbf{r}) . \quad (2.3)$$

Here, $V_{\rm ion}$ is the sum of the hydrogen and carbon ion core potentials, V_H is the Hartree potential due to the valence charge density $\rho(\mathbf{r})$, and $\mu_{{\rm xc},\sigma}(\mathbf{r})$ is the exchange-correlation potential for electrons of spin σ. The valence charge density is given by

$$\rho(\mathbf{r})=e\sum_{i,\sigma}^{\rm occ}|\psi_{i,\sigma}(\mathbf{r})|^2=\rho_\uparrow(\mathbf{r})+\rho_\downarrow(\mathbf{r}) . \quad (2.4)$$

In this equation, the sum extends over all occupied states and both spin directions. $E_{\rm tot,el}$ can be obtained from

$$E_{\rm tot,el}=\sum_{i,\sigma}^{\rm occ}\varepsilon_{i,\sigma}-\frac{1}{2}\int V_H(\mathbf{r})\rho(\mathbf{r})d\mathbf{r} +\sum_\sigma\int[\varepsilon_{{\rm xc},\sigma}(\mathbf{r})-\mu_{{\rm xc},\sigma}(\mathbf{r})]\rho_\sigma(\mathbf{r})d\mathbf{r} , \quad (2.5)$$

where $\varepsilon_{{\rm xc},\sigma}(\mathbf{r})\rho_\sigma(\mathbf{r})$ is the exchange-correlation energy density for spin σ. Equation (2.5) accounts for overcounting of the Coulomb interaction between the electrons in the sum of eigenvalues. Because of the long-range nature of the Coulomb potential, the potentials $V_H(\mathbf{r})$, $V_{\rm ion}(\mathbf{r})$, and the energy $E_{\rm core\text{-}core}$ contain infinite contributions which cancel with one another and can be excluded explicitly in a plane-wave basis.

Equation (2.1) gives the total energy of the solid for a given ionic configuration, i.e., fixed positions of the ions in the unit cell. It implicitly invokes the adiabatic approximation. In order to optimize the structures, we have also computed the total Coulombic force exerted on the ions, employing the momentum-space expression for the Hellman-Feynman theorem, as derived by Ihm *et al.*[57] The positions of the ions in the unit cell have been determined by an iterative procedure consisting of the following steps: (1) perform a self-consistent calculation of the total energy of the system with fixed ionic positions; (2) calculate the force exerted by the electrons on the ions, and shift the ions by a small amount in the direction of this force; (3) go back to step (1) until the ions are in equilibrium with the electrons.

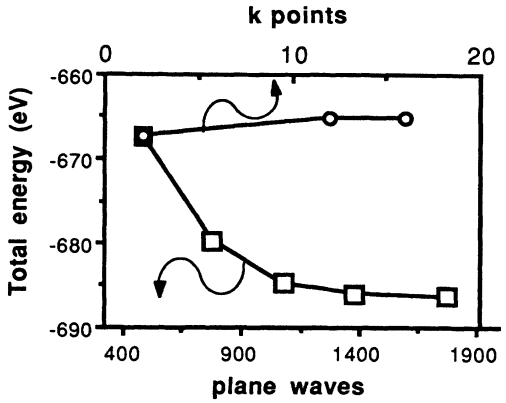

FIG. 1. Convergence of the calculated total crystal energy per unit cell as a function of the number of plane waves included in the Hamiltonian matrix, and as a function of the number of special **k** vectors (Ref. 77) included in the integrals of the charge density and the electronic potential over the irreducible wedge of the Brillouin zone.

For the $P2_1/a$ and $P2_1/n$ structures of *trans*-$(CH)_x$ which are specified in Sec. II B, we have solved Eq. (2.3) with 1800 plane waves as basis states (corresponding to a maximum kinetic energy of 35 Ry). We used up to 16 special **k** points[77] in an irreducible part of the Brillouin zone for the **k** integrations and 1024 special **r** points in an irreducible part of the unit cell for the real-space integrations. Approximately 10–20 iterations were needed to obtain total energies converged to within 1 meV. The convergence in the total energy is illustrated in Fig. 1 for *trans*-$(CH)_x$ in the $P2_1/a$ structure.

B. Characterization of the three-dimensional structure of *trans*-$(CH)_x$

Recent experimental structural data indicate that *trans*-$(CH)_x$ has a monoclinic unit cell with $P2_1/c$ symmetry.[21] The unit cell contains two transplanar C_2H_2 chain units, with one shorter and one longer carbon-carbon bond in each chain corresponding to a dimerized structure. The precise relationship between the two polyacetylene chains in the unit cell is still controversial. Two possible configurations, consistent with the space group $P2_1/c$, have been proposed: (1) an inphase[34] ($P2_1/a$) and (2) an antiphase arrangement[18] ($P2_1/n$) of the dimerized backbone. In Figs. 2 and 3 we depict the unit cell of *trans*-$(CH)_x$ in the $P2_1/a$ and $P2_1/n$ structures, respectively.

The two structures, $P2_1/a$ and $P2_1/n$, are difficult to distinguish from the intensity of x-ray reflections. For structures with bond alternations in phase, all the (00*l*) in-chain x-ray reflections are allowed, while only even *l* reflections are allowed for $P2_1/n$ structures with bond alternations out of phase. The (001) and (003) reflections were clearly observed in highly oriented nonfibrous Durham-Graz *trans*-$(CH)_x$ material,[34] indicating the $P2_1/a$ structure, whereas these reflections were either not

TABLE I. Cartesian coordinates of atoms in *trans*-$(CH)_x$. The y and z directions are chosen along the b and c axes, respectively. The x direction is then *approximately* along the a axis. We tabulate only the positions of the four atoms on one chain in the unit cell and, additionally, of one carbon atom on the second chain, since this differs in the $P2_1/a$ and $P2_1/n$ structure. The other atomic coordinates then follow from symmetry. The numerical values of the structural parameters are given in Table II.

Atom	x coordinate	y coordinate	z coordinate
C(1)	$\frac{p}{2}\sin\phi_C$	$\frac{p}{2}\cos\phi_C$	$\frac{c}{4}-\frac{u_C}{2}$
H(1)	$\left[\frac{p}{2}+(l_{C\text{-}H}^2-u_H^2)^{1/2}\right]\sin\phi_H$	$\left[\frac{p}{2}+(l_{C\text{-}H}^2-u_H^2)^{1/2}\right]\cos\phi_H$	$\frac{c}{4}-\frac{u_C}{2}-u_H$
C(2)	$-\frac{p}{2}\sin\phi_C$	$-\frac{p}{2}\cos\phi_C$	$\frac{3c}{4}+\frac{u_C}{2}$
H(2)	$-\left[\frac{p}{2}+(l_{C\text{-}H}^2-u_H^2)^{1/2}\right]\sin\phi_H$	$\left[\frac{p}{2}+(l_{C\text{-}H}^2-u_H^2)^{1/2}\right]\cos\phi_H$	$\frac{3c}{4}+\frac{u_C}{2}+u_H$
$P2_1/a$:C(3)	$\frac{p}{2}\sin\phi_C+\frac{a}{2}\sin\beta$	$-\frac{p}{2}\cos\phi_C+\frac{b}{2}$	$\frac{c}{2}-\frac{u_C}{2}+\frac{a}{2}\cos\beta$
$P2_1/n$:C(3)	$-\frac{p}{2}\sin\phi_C+\frac{a}{2}\sin\beta$	$\frac{p}{2}\cos\phi_C+\frac{b}{2}$	$\frac{c}{2}+\frac{u_C}{2}+\frac{a}{2}\cos\beta$

seen or were observed to decrease following various electrochemical treatments in *trans*-polyacetylene.[18,78] The rocking curves in the highly oriented Durham-Graz material[34] indicate a much better alignment of the polymer chains (5° in Ref. 34 compared to approximately 10° in Ref. 78) and show an intensity ratio of the (001) to (002) reflections which is in accord with the theoretically expected value.[78] In sum, we expect that Durham-Graz experiments reflect intrinsic properties of crystalline *trans*-$(CH)_x$ more faithfully, since samples with significantly better aligned chains were used and the x-ray reflections characteristic for the $P2_1/a$ structure could be quantitatively identified.[34]

In order to characterize completely either of these two structures, the following structural constants need to be known: the lattice constants a, b, and c, the monoclinic angle β between a and c, two setting angles ϕ_C and ϕ_H between the plane containing the carbon and hydrogen chain, respectively, and the b axis, the projection p of the C-C distance within a chain onto the a-b plane, the distance $l_{C\text{-}H}$ between the carbon and hydrogen atoms within a chain, the dimerization amplitude $u_C=\pm 2u_0$ of the C—C bonds in the c direction, and the displacement u_H of the hydrogen atoms relative to their adjacent carbon atom.[27,34] In Table I the positions of the atoms in the unit cell are specified in terms of these parameters for both $P2_1/a$ and $P2_1/n$ structures of *trans*-polyacetylene. The experimental values are summarized in Table II.

C. Results of the three-dimensional local-density approach

1. Total energy and relative stability of $P2_1/n$ and $P2_1/a$

In this section we will present our theoretical results for the structural total energies and optimized lattice parameters. Initially, we have used the experimentally established lattice parameters shown in Table II and performed spin-unpolarized, self-consistent LDA electronic-structure calculations in the two competing structures. As indicated in Table III, using these experimental parameters, our calculations show that the $P2_1/a$ structure is lower in total energy by an amount of 0.01 ± 0.003 eV per $(C_2H_2)_2$ unit. This difference is consistent with the similarity of the two structures, and is of the order of optical phonon energies in solids. As we shall later demonstrate, the greater stability of the $P2_1/a$ phase relative to the $P2_1/n$ phase has a clear physical origin: namely, a (weak) chemical bonding caused by overlaps between carbon and hydrogen orbitals on adjacent chains in the unit cell. These overlaps are more pronounced in the $P2_1/a$ phase.

Since the self-consistent value of the dimerization u_C will be an important issue in our later discussion, it is important to stress that, irrespective of the precise value of u_C, our results show that the dimerized $P2_1/a$ structure is *lower* in total energy than the dimerized $P2_1/n$ structure. This is illustrated in Table III. For the calculated force-free value ($u_C=0.01$ Å) it is 0.007 eV, whereas for zero bond alternation it is 0.030 eV. The increased stability of the $P2_1/a$ structure relative to the $P2_1/n$ structure as the dimerization goes to zero has the same physical

TABLE II. Experimental and predicted structure parameters for crystalline *trans*-polyacetylene. The parameters are defined in the text and Table I.

Structure parameters	Expt.	Present calc.
a (Å)	4.18	
b (Å)	7.34	
c (Å)	2.455	
β (deg)	90.5	
ϕ_C (deg)	57	55.1
ϕ_H (deg)	57	57.0
p (Å)	0.68	0.64
u_C (Å)	0.052	0.01
$l_{C\text{-}H}$ (Å)	1.09	1.12
u_H (Å)	0.025	0.04

TABLE III. Relative stability of the two monoclinic structures of *trans*-polyacetylene. The difference in the calculated total energy per cell in the $P2_1/a$ structure and the $P2_1/n$ structure is listed. The corresponding structural lattice parameters are given in Table II; the undimerized structural data imply $u_C=0$ and $u_H=0$ and $\beta=90°$.

Structure data	$E_{tot}(P2_1/a)-E_{tot}(P2_1/n)$
Experimental	−0.010
Optimized	−0.007
Undimerized	−0.030

origin as the overall energy difference, since for $u_C \to 0$ one can see that the overlapping carbon and hydrogen orbitals are brought into closer alignment.

Several qualitative arguments have been advanced in favor of one or the other structure for crystalline *trans*-CH_x. On the basis of the tight-binding SSH model,[17] including (constant) interchain hopping matrix elements, it was found[35] that an *alternating* dimerization on neighboring chains as in the $P2_1/n$ structure is energetically favorable, provided there is particle-hole symmetry.[35] Alternatively, if one allows the interchain hopping integrals to alternate in sign, then one can argue[37] that the $P2_1/a$ structure is favored. In Sec. II C 4 we shall present detailed arguments establishing that there is significant interchain (chemical) bonding interaction between carbon and hydrogen atoms which violates particle-hole symmetry and causes the $P2_1/a$ structure to be favored. Each H atom on one chain approximately points towards a carbon p orbital on one of the neighboring chains. These adjacent atoms are shown in Figs. 2 and 3 by dashed lines. The distance between the H atom on one chain and its nearest carbon neighbor on another chain is 2.9 Å in the $P2_1/a$ structure and 3.1 Å in the $P2_1/n$ structure. This difference provides a crucial additional bonding energy that favors the $P2_1/a$ structure. In addition, the distance between the adjacent carbon and hydrogen atoms decreases slightly with decreasing dimerization, which causes the trends in Table III.

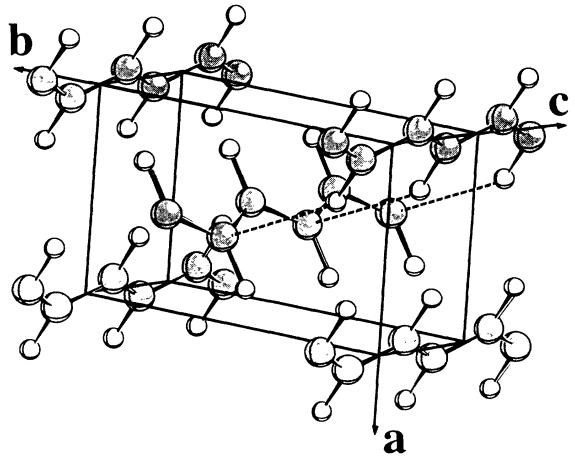

FIG. 2. Conventional unit cell of *trans*-$(CH)_x$ in the $P2_1/a$ structure. The dashed lines are drawn to emphasize a characteristic feature of this structure: the hydrogen atoms of one chain point approximately towards the carbon atoms of the neighboring chains.

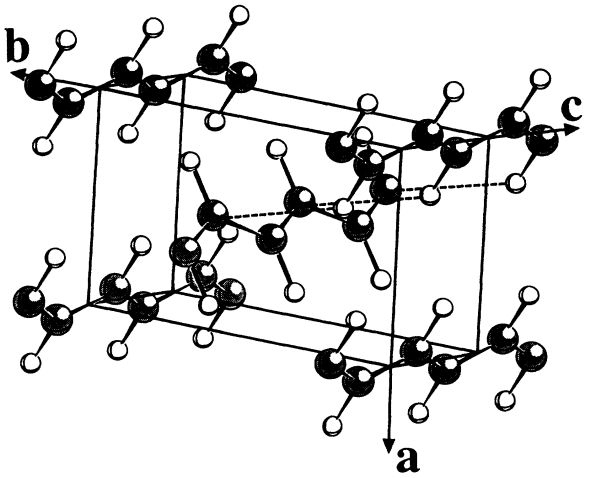

FIG. 3. Conventional unit cell of *trans*-$(CH)_x$ in the $P2_1/n$ structure. As in Fig. 2, the dashed lines emphasize the approximate alignment of the carbon and hydrogen atoms on adjacent chains. However, these atoms are further apart in the $P2_1/n$ structure than in the $P2_1/a$ structure.

2. *Optimized ion positions in the unit cell*

In this subsection we present results from the computation of the Hellmann-Feynman forces and the corresponding iterative optimization of the ion positions within the unit cell.

In Fig. 4 we depict some typical results for the forces and corresponding changes in two of the lattice parameters, u_C and u_H. In the middle of the figure we show the total energy, which is lowered by each iteration. Each iteration represents a self-consistent electronic-structure calculation. Corresponding to the lowering of the total energy, the forces exerted on the ions decrease. The resulting lattice parameters are summarized in Table II and compared to the experimental values. We note that we have used the experimental values for the lattice constants a, b, c, and β, since these data are accurately established experimentally and their theoretical determination would require calculation of the full stress tensor. We find our predicted setting angles, the zig-zag amplitude of the C chains, and the C-H distance to be very close to the experimental values. We find a buckling of the carbon-hydrogen plane, which is apparently small in the case of *trans*-$(CH)_x$. To our knowledge, such a buckling has not been discussed so far in the literature on polyacetylene.

A considerable discrepancy between theory and experiment, however, is the small dimerization u_C predicted by the present theory. This finding is consistent with recent first-principles calculations of u_C both for single chains[41,43–45] and for 3D structures.[42,52,79,80] Although it is conceivable that the dimerization in perfect crystalline all *trans*-$(CH)_x$ is somewhat smaller than in the majority of the available samples, in view of the large

difference between the theoretical prediction and the accepted experimental value, a discrepancy between theory and experiment is likely to remain. In this regard, however, it is first important to emphasize that our results do predict unambiguously that u_C is *nonzero*. The evaluation of the Hellmann-Feynman forces proved crucial for our calculation of u_C, since they are an order of magnitude more sensitive to u_C than the total energy itself; because of this effect, other total energy studies were either unable to obtain unambiguous results for u_C (Ref. 42) or concluded that it was zero (Ref. 80).

The most plausible origin of such discrepancy is in the LDA itself, i.e., in a correlation effect which is not fully captured by the method in either the 1D or the 3D calculations. Recently, it was suggested[80] that this theoretical underestimate of dimerization could be linked to the inadequate treatment of correlation effects in LDA, since more exact methods have established that for one-dimensional models the proper inclusion of correlation effects *enhances* dimerization for weak *e-p* coupling.[81–85]

In view of the importance of this uncertainty in the value of u_C, we have checked all major results of this paper both with the force-free set of structural parameters—as shown in Table II—and with the experimental set of parameters. Fortunately, none of the major physical conclusions in our analysis depends sensitively on the value of u_C.

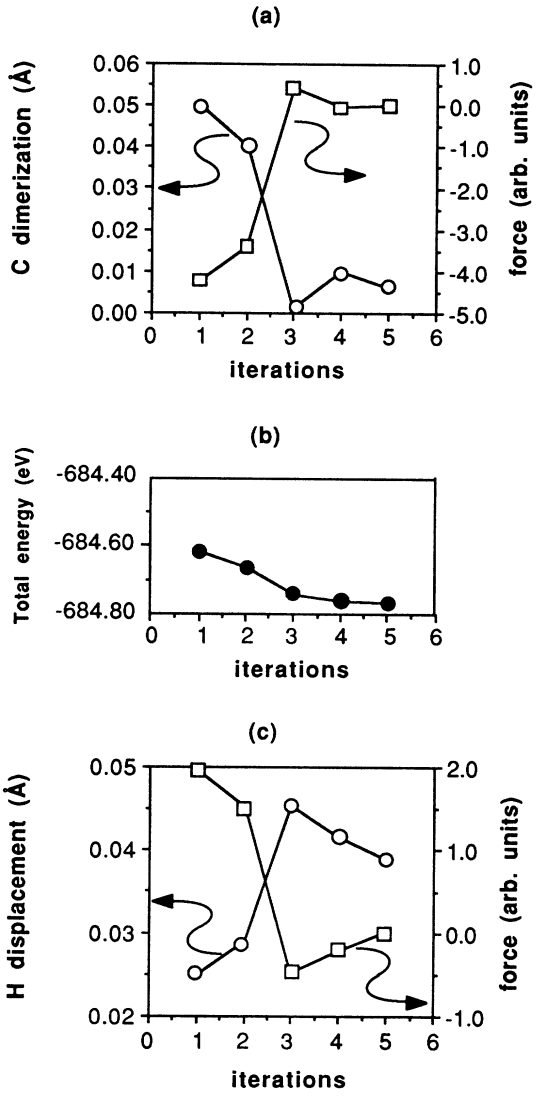

FIG. 4. Convergence of calculated structural parameters. Each iteration corresponds to a complete self-consistent total electronic energy calculation for a given configuration of the ions in the unit cell. Shown are the Hellmann-Feynman forces on the carbon [panel (a)] and the hydrogen atoms [panel (c)] and the corresponding value of dimerization which minimizes the total electronic energy. The total crystal energy decreases with each iteration [panel (b)], as the ions and electrons are being brought into better equilibrium with respect to one another.

3. *Spin polarization in the ground state*

We have already mentioned that the spin-unpolarized local-density-functional approach inevitably loses some of the true correlation effects that occur in spin-unsaturated many-electron systems such as *trans*-$(CH)_x$. As demonstrated by many examples (see Sec. II A), a substantial portion of these correlations can be captured by the local-spin-density method (LSDA).[76]

We have therefore minimized the total energy of *trans*-$(CH)_x$ in the $P2_1/a$ phase in the LSDA. In the calculation, we start with an initial spin polarization by artificially spin polarizing the ion potentials in the unit cell. The effective one-particle equation (2.3) is then solved iteratively until the potential and resulting valence charge and spin density are self-consistent. After a few iterations, the spin polarization is concentrated on the C π orbitals. Finally, however, it tends to zero, and a spin-unpolarized ground-state results. Consequently, the spin-density-functional theory predicts that 3D crystalline *trans*-$(CH)_x$ has no (antiferromagnetic) Mott ground state at $T=0$.

4. *Electronic charge density*

The chemical bonding within the $(CH)_x$ chains and between the chains may be examined by computing the electron charge density. In this section we discuss the calculated valence electron charge density in *trans*-$(CH)_x$ in the $P2_1/a$ structure. The geometry of the three planes in the unit cell in which we shall depict the charge density is shown in Fig. 5. The structural parameters we have used are listed in the second column of Table II. Figures 6 and 7 depict the total valence charge density. The pronounced maxima between the carbon atoms in Fig. 6 reflect the strong σ bonding of the carbons along the c axis.

The perhaps most striking results are contained in Figs. 8 and 9. They show the electron charge density distribution in the two uppermost valence bands (Fig. 8) and the two lowest conduction bands (Fig. 9), respectively. According to the standard SSH model,[17] these figures should be identical, apart from a small bonding charge between the carbon atoms: that is, in the SSH model, these bands are simply bonding and antibonding com-

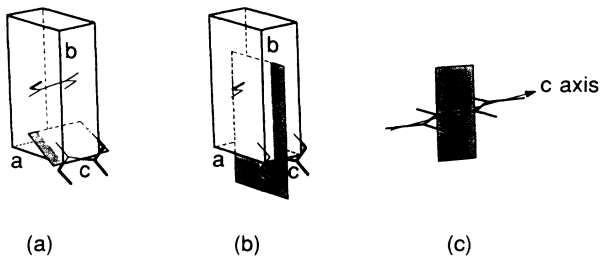

FIG. 5. The computed electronic charge density surfaces in the following figures refer to one of the plane sections of the unit cell shown here: (a) the plane of the carbon-hydrogen σ bonds. (b) The plane perpendicular to that shown in (a) and parallel to the carbon-hydrogen bond in one chain. This plane section displays the carbon π bonds and also illustrates the charge distribution between the chains. (c) The plane perpendicular to that shown in (a) and parallel to the carbon-carbon bond.

binations of the molecular π orbitals and hence obey particle-hole symmetry.

The first-principles calculations show that these states are indeed primarily molecular π bands consisting mainly of carbon p orbitals. This is particularly evident from Fig. 10, which shows the characteristic lobes of a p-wave function. Importantly, however, in contrast to a one-dimensional picture such as the SSH model, the top valence band states in crystalline *trans*-$(CH)_x$ (Figs. 8 and 10) consist of a mixture of hydrogen and carbon states, whereas the bottom conduction states are essentially pure carbon states (Fig. 9). This asymmetry in the valence and conduction states is a consequence of an additional bonding mediated by the interaction of carbon states and hydrogen states across the chains (see Fig. 2). We have repeated our calculations with larger lateral lattice constants a and b and find that this asymmetry and the hydrogen contribution in the top valence bands disappear when a and b are increased by more than 30%.

Quite recently, it has been argued[86] that the "bond-charge" repulsion between electrons in the π orbitals between the carbon atoms could be physically significant and could alter the manner in which the e-e interactions should be modeled in polyacetylene and other conducting polymers.[86] In a naive tight-binding picture, one might expect at least a weak "buildup" of charge between the two carbon atoms linked by a double bond. In Fig. 11 we show that the actual charge density does not indicate any such buildup between these carbons atoms; indeed, the charge density is pealed primarily around the atomic sites and is rather insensitive to the extent of the dimerization.

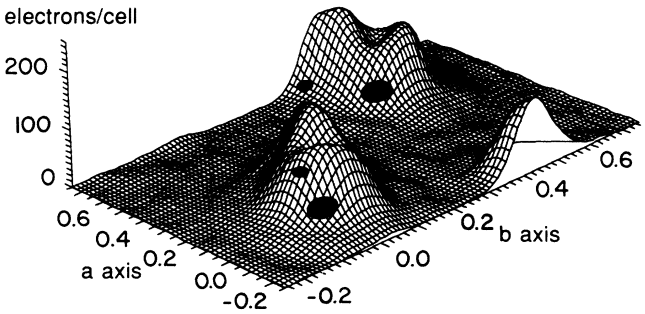

FIG. 7. Calculated total electronic valence charge density in the plane shown in Fig. 5(b). The large and small black circles show the projected positions of the carbon atoms and hydrogen atoms onto the a-b plane, respectively.

5. *Band structure*

In Figs. 12, 13, and 14 we show, respectively, the electronic band structure for the dimerized $P2_1/a$ and $P2_1/n$ phases and (for completeness, the unphysical) undimerized $P2_1/a$ phase of crystalline *trans*-$(CH)_x$ that follows from the self-consistent LDA calculations using the structural parameters listed in the second column of Table II. These figures show that in both structures the interchain interactions alter crucially the symmetry and dimensionality of the band states close to the minimum gap. Significantly, in view of the underestimate of the dimerization in the force-free parameters, comparison of Figs. 12 and 14 shows that these band-edge splittings

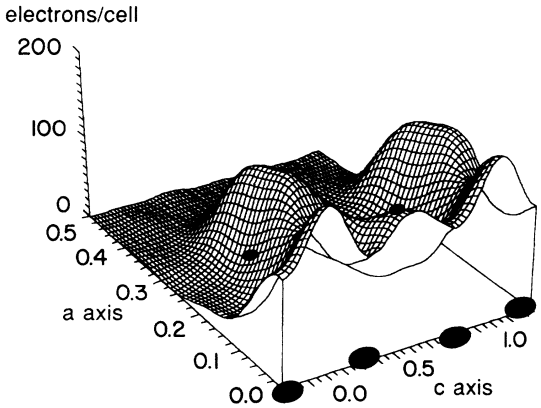

FIG. 6. Calculated total electronic valence charge density in the plane shown in Fig. 5(a). The large and small black circles show the projected positions of the carbon atoms and hydrogen atoms onto the plane depicted in Fig. 5(a), respectively.

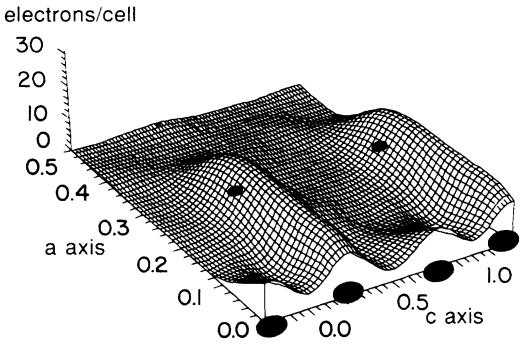

FIG. 8. Calculated electronic valence charge density associated with the two uppermost valence bands (conventionally called "π" bands). The plotted charge surface lies in the plane shown in Fig. 5(a).

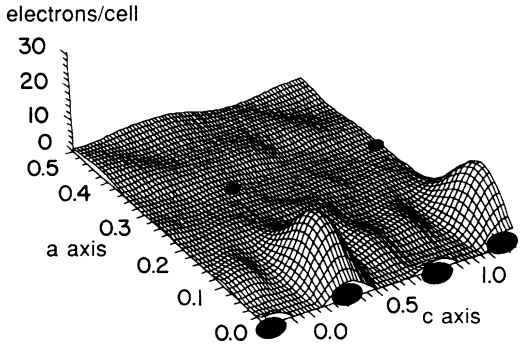

FIG. 9. Calculated electronic valence charge density associated with the two lowest conduction bands (conventionally called "π^*" bands). The plotted charge surface lies in the plane shown in Fig. 5(a). The difference between Figs. 8 and 9 originates in the coupling of carbon and hydrogen atoms across neighboring chains; it demonstrates the broken particle-hole symmetry.

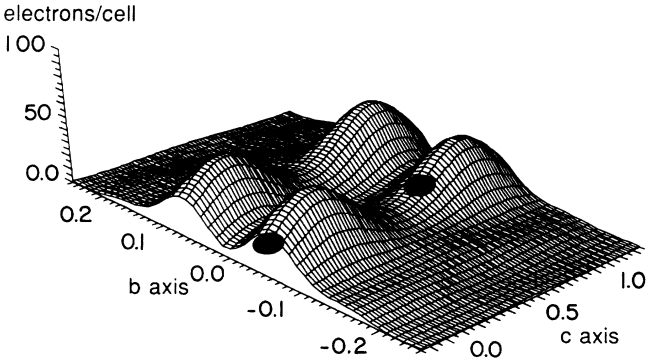

FIG. 11. Calculated valence charge density associated with the two uppermost valence bands (conventionally called "π" bands). The plotted charge surface lies in the plane shown in Fig. 5(c). This figure shows the weak bonding of the carbon π states. The large and small black circles show the projected positions of the carbon atoms and hydrogen atoms onto the plane depicted in Fig. 5(c), respectively.

near the minimum gap (around **k** point k_B) are insensitive to the value of the dimerization. Since these band-edge states play an essential role both for low-lying excitations and in the formation of intrinsic defects (see Sec. III below), these observations are most significant.

As discussed in Sec. II A, the one-particle spectrum differs from the LDA band structure to a very good level of approximation by a wave-vector-independent self-energy correction Σ_{el}, which raises the energy of the conduction bands. We have estimated this self-energy by comparing the calculated combined density of states of *trans*-$(CH)_x$ in the $P2_1/a$ structure with the experimental optical-absorption spectrum (see Sec. II C 7) and find $\Sigma_{el}=0.74$ eV. This self-energy is included in the Figs. 12, 13, 15, and 16 to facilitate a comparison between theory and experiment.

Let us first discuss the band structure in the $P2_1/a$ phase, shown in Fig. 12. The pair of the two highest valence and lowest conduction bands are *mainly* carbon-π orbital derived states and show, overall, *approximate* particle-hole symmetry. If there were no interchain interaction, all energy bands would be twofold degenerate throughout the Brillouin zone, reflecting the two C_2H_2 chain segments in the unit cell. This is illustrated in Fig. 15(b). In the same limit, the minimum gap would be pro-

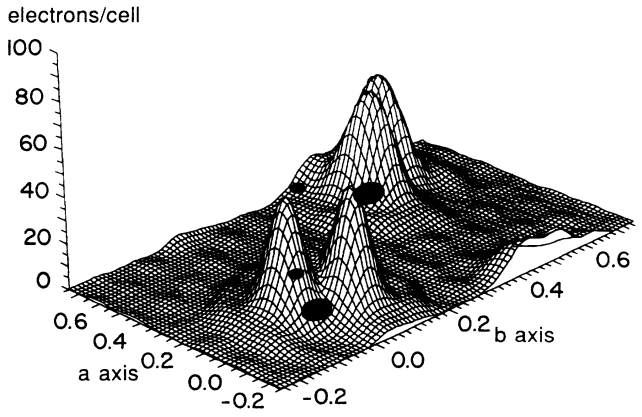

FIG. 10. Calculated valence charge density associated with the two uppermost valence bands (conventionally called "π" bands). The plotted charge surface lies in the plane shown in Fig. 5(b). This figure exhibits the characteristic π lobes associated with the nonbonding carbon π states.

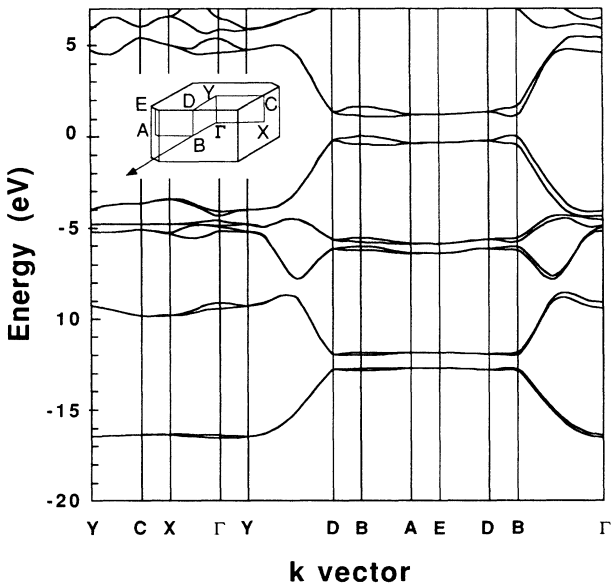

FIG. 12. Predicted electronic band structure of *trans*-$(CH)_x$ in the $P2_1/a$ structure. The zero of energy has been chosen to lie within the energy gap. The dimerization has been set to the experimental value of $u_C=0.05$ Å; the other structural parameters have been optimized self-consistently (see Table II). The conduction bands include a k-independent self-energy correction of $\Sigma_{el}=0.74$ eV (see discussion in Sec. II C 5). The insert shows the three-dimensional Brillouin zone; the chain axis is marked by an arrow.

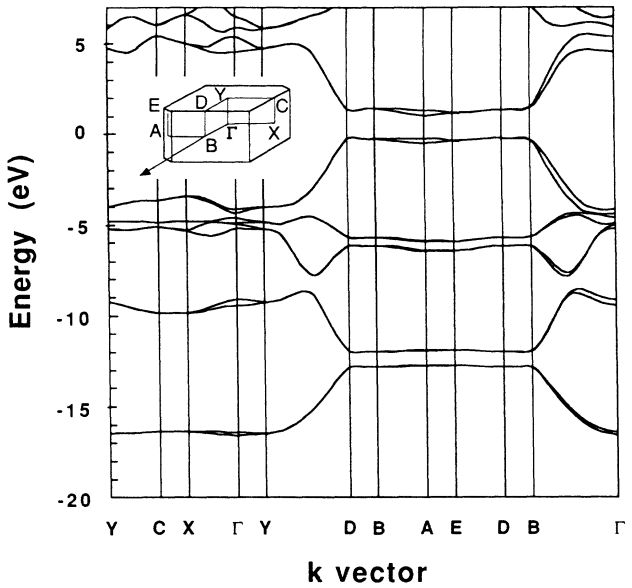

FIG. 13. Predicted electronic band structure of *trans*-$(CH)_x$ in the $P2_1/n$ structure. The zero of energy has been chosen to lie within the energy gap. The dimerization has been set to the experimental value of $u_C=0.05$ Å; the other structural parameters have been optimized self-consistently (see Table II). The conduction bands include a **k**-independent self-energy correction of $\Sigma_{el}=0.74$ eV (see the discussion in Sec. II C 5). The insert shows the three-dimensional Brillouin zone; the chain axis is marked by an arrow.

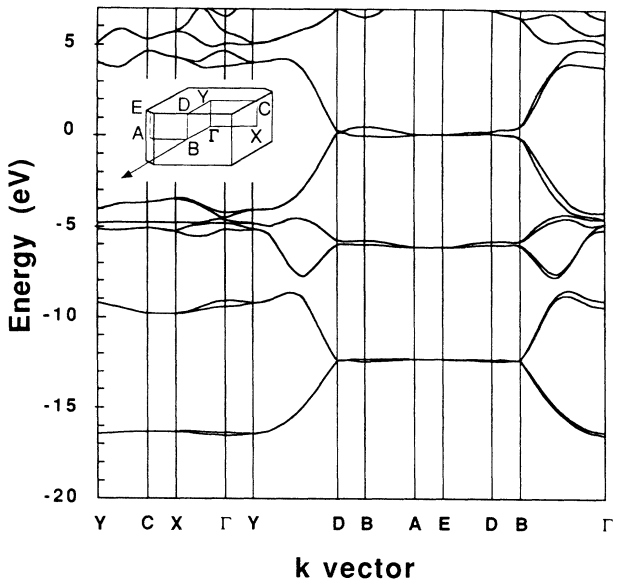

FIG. 14. Calculated electronic band structure of *trans*-$(CH)_x$ in a hypothetical $P2_1/a$ structure with zero dimerization. The zero of energy has been chosen to lie within the energy gap. since the dimerization has been set to zero, this does not correspond to the experimental situation.

portional to the dimerization and would consequently vanish for zero dimerization at any of the **k** points k_D, k_B, k_A, and k_E at the boundary of the Brillouin zone. Our first-principles calculations show, on the contrary, that the bands in three-dimensional *trans*-$(CH)_x$ behave differently close to the Fermi level. As indicated in Fig. 15, the pairs of the two lowest conduction and highest valence bands near the **k** point $B=(0,0,\frac{1}{2})$ are split by 0.53 eV and 0.46 eV, respectively. With decreasing dimerization, $u_C\rightarrow 0$, these splittings decrease, but the gap between conduction and valence band remains finite near k_B, as can be seen in Fig. 14 for the undimerized structure.

The minimum band gap in the $P2_1/a$ phase is found to be slightly indirect, as shown in Fig. 15. The valence-band maximum lies at $\mathbf{k}=(0,\frac{1}{8},\frac{1}{2})$, whereas the minimum conduction band edge occurs at $\mathbf{k}=(\frac{1}{4},0,\frac{1}{2})$.

In a tight-binding framework, one can very crudely estimate the strength of the interchain coupling from its effect of the band structure. Equating the width of the splitting in the band-edge states near the **k** point k_B to $4t_\perp$, we obtain an effective interchain hopping matrix element $t_\perp=0.12$ eV, compared to $t_\parallel=2.5$ eV for the intrachain coupling matrix element. These values are roughly consistent with experimental anisotropy factors of the order of 100 in the conductivity,[53] since the ratio of transverse to longitudinal conductivity is proportional to $(t_\perp/t_\parallel)^2$. A tight-binding analysis of optical experiments in *trans*-$(CH)_x$ under pressure[87] has led to estimates for $4t_\perp=0.3$ eV, which is also consistent with our first-principles results. The interchain effects are very sensitive to crystalline order; by increasing the distance between the two chains by 5%, the splittings in the band-edge states decrease by 31%, in accord with the previously discussed charge-density results. The band splittings are also weaker in the $P2_1/n$ structure (see Fig. 13), since the distance between the neighboring C and H atoms is larger in this case.

Turning next to our results for the $P2_1/n$ band structure which are shown in Fig. 13, we find that they are in general agreement with prior first-principles calculations

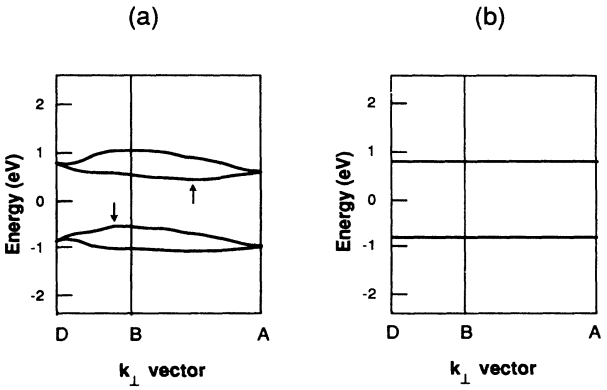

FIG. 15. (a) Predicted electronic band structure of *trans*-$(CH)_x$ in the $P2_1/a$ structure near the fundamental energy gap. The arrows indicate the position of the top of the valence band and the bottom of the conduction band, respectively. (b) Same within an idealized 1D tight-binding band model [SSH model (Ref. 17)].

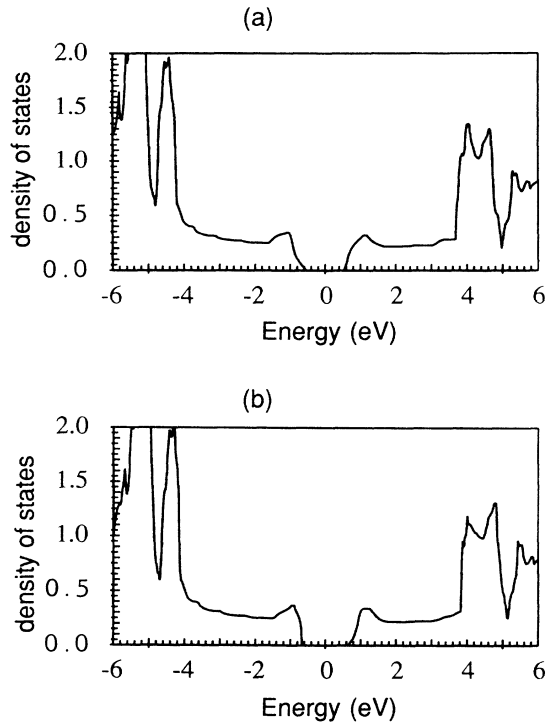

FIG. 16. Predicted electronic density of states of *trans*-$(CH)_x$ (a) in the $P2_1/a$ structure and (b) in the $P2_1/n$ structure. The zero of energy lies in the middle of the energy gap.

of Grant and Batra[28–30] and of Ashkenazi and coworkers.[31,32,42,80] There are some differences in the conduction bands which are likely to originate in differences in the method, numerical details, and atomic positions. The present results are more accurate than those of Refs. 28–30 in the sense of (apparent) numerical convergence. Grant and Batra[30] included 500 plane waves, whereas we included more than 1800 and employed a more accurate soft-core norm-conserving pseudopotential. Ashkenazi *et al.*[31] used the linear muffin-tin orbitals method in the atomic-sphere approximation (LMTO-ASA) which approximates the crystal potential by muffin tins and neglects the intermediate regimes. This is quite adequate for close-packed structures but represents a fairly drastic approximation in an open, highly anisotropic structure such as *trans*-$(CH)_x$. The present calculations contain no approximations to the shape of the crystal potential.

We note that Grant and Batra[30] did not include the wave vectors close to the **k** point $\mathbf{k}_A=(-\frac{1}{2},0,\frac{1}{2})$ (see Fig. 13) in their published band structure; since the interchain interaction shows up significantly only for this **k** vector, they concluded prematurely that the band splitting induced by three-dimensional effects is smaller than 0.1 eV close to the Fermi energy; at the wave vector $\mathbf{k}_A$, we obtain a splitting of 0.23 eV for the topmost valence bands in the $P2_1/n$ structure.

A significant modification of the band states close to the Fermi energy by interchain interactions was also found by Ashkenazi *et al.*[42] A sufficiently large interchain coupling reduces the energy gained by the formation of a dimerized ground state and favors a metallic ground state with no bond alternation. It was therefore argued in Ref. 42 that the interchain interaction could, in fact, be partly responsible for the small bond alternation predicted by the LDA. The recent calculations of Mintmire and White[41] indicate, however, that the local-density-functional method predicts the same small dimerization u_C even in one-dimensional $(CH)_x$ chains. In this regard we note that our calculations, which optimize the atomic positions in both $P2_1/a$ and $P2_1/n$ *trans*-$(CH)_x$, predict the same value for u_C in both structures, even though the interchain coupling is substantially weaker in $P2_1/n$ polyacetylene.

6. *Interchain electron-phonon interaction*

To explore further the coupling of electronic and ionic motions—in particular the interchain electron-phonon interaction—we start from the undimerized $P2_1/a$ structure with all carbon bond lengths being equal (Fig. 14). When every other carbon atom (and its accompanying hydrogen atom) is displaced along the chain axis by a small amount $\pm u_0$, an energy gap opens between valence and conduction bands. In the ground state of the $P2_1/a$ structure, the dimerizations on neighboring chains are in phase. We can, instead, consider a small *out*-of-phase bond alternation on neighboring chains which can be thought of as a long-wavelength phonon with its **q** vector *perpendicular* to the chain direction. In the limit of no interchain interaction, the changes in the energy bands induced by the in-phase and out-of-phase atomic displacements on neighboring chains should be identical.

The calculations show that in the actual crystalline *trans*-$(CH)_x$ the electron-phonon interaction mediated by the interchain bonding causes the in- and out-of-phase displacements to differ significantly. Figure 17 depicts self-consistent energy bands for a small in-phase dimerization [Fig. 17(a)] and a small out-of-phase dimerization [Fig. 17(b)] and clearly shows the strong influence of interchain effects.

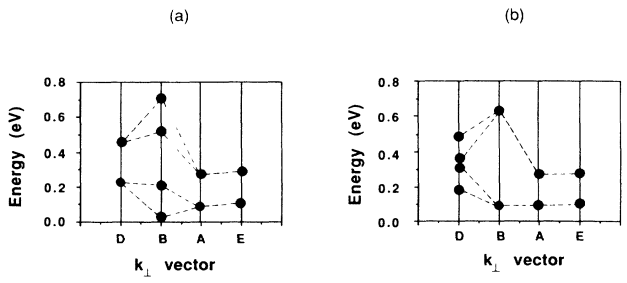

FIG. 17. Predicted electronic deformation potentials (band-edge energies) for (a) an in-phase dimerization of $u_C=0.01$ Å in the $P2_1/a$ structure on every chain and (b) an out-of-phase dimerization of $u_C=0.01$ Å on neighboring chains. Shown are the two uppermost valence and two lowest conduction bands for electronic wave vectors perpendicular to the chain direction (cf. Fig. 12). This figure illustrates the marked influence of the interchain interaction on the electronic states near the energy gap.

The pronounced **k** dependence of these interchain effects strongly indicates that the dominant interaction across the chains is *not* of the Van der Waals type but is rather a chemical bonding (i.e., electron-ion interaction).

7. *Density of states in three-dimensional trans-$(CH)_x$*

Since the density of states is related to a number of experimental observables, it is obviously an important quantity to calculate in any theoretical study. In Fig. 16(a) we show the density of states predicted by our LD calculations for *trans*-$(CH)_x$ in the $P2_1/a$ structure. For purposes of comparison with both other theoretical results and with experiments, we also plot in Fig. 16(b) the density of states predicted for *trans*-$(CH)_x$ in the $P2_1/n$ structure. Recall that in an idealized one-dimensional system, the density of states is singular at the band edges and varies as $(E-E_{\rm gap})^{-1/2}$ for energies E close to the band edge. In a three-dimensional system, the density of states remains regular for all energies and varies as $(E-E_{\rm gap})^{1/2}$ near the band edge. The band structure displayed in Figs. 12 and 13 is reflected in the density of states in Fig. 16. In particular, the interchain coupling which leads to the (approximately symmetric) splitting of the topmost valence and lowest conduction bands in Figs. 12 and 13 produces in Fig. 16 a broadening of the 1D singularity in the density of states. The resulting band-edge density of states shows an onset which is characteristic of 3D systems. Further, despite some asymmetries near the band edge, the overall densities of states in the π and π^* bands are fairly similar, reflecting the approximate particle-hole symmetry that was also apparent in the band structures of Figs. 12 and 13.

Possible experimental probes of these density of state predictions include x-ray photoemission spectroscopy (XPS), ultraviolet photoemission spectroscopy (UPS), and electron-energy-loss spectroscopy (EELS) measurement. A recent EELS study[88] of *trans*-$(CH)_x$ confirms the rough particle-hole symmetry but does not have sufficient resolution to permit a detailed comparison with our results near the minimum gap. Optical absorption data on π-π^* transitions can provide information on the *joint* density of states, although in the present case there are two difficulties in making any precise comparisons between theory and experiment. First, at a general level, optical absorption involves not only the joint density of states but also a matrix element. However, near the band edge, we expect that this matrix-element effect is relatively slowly varying and that the transition rate for optical absorption is proportional to the joint density of states. Second, as discussed above, a direct comparison between the LDA calculations and the experimental data is not meaningful, since the local-density method does not give the correct optical gap. Since, however, previous calculations in semiconductors have shown that the major difference between the LDA band structure and the optically excited quasiparticle states is a rigid shift $\Sigma_{\rm el}$ of the conduction bands, by performing this shift we can compare the calculated *structure* of the joint density of states with the experimental data and study the 3D effects on the optical absorption. With these two caveats, we can proceed to a comparison of the joint density of states with the optical-absorption data.

Experimentally, the optical band-gap absorption in *trans*-polyacetylene has been investigated in a number of papers.[53,87,89–93] Detailed measurements in Shirakawa material were carried out by Fincher *et al.*[89] and clearly exhibited the quasi-one-dimensional character of $(CH)_x$. However, the 1D singularity in the gap absorption was substantially broadened and an extended tail at the onset of absorption was observed. The steep portion in the absorption spectrum led to a direct "one-dimensional" gap $E_{\rm gap}^{\rm 1D}$ of 1.4 eV, while the absorption tail was attributed to a three-dimensional interchain coupling. Fincher *et al.*[89] concluded that *trans*-polyacetylene has an indirect "three-dimensional" gap $E_{\rm gap}$ of about 1.1 eV. A later analysis of optical data in *trans*-$(CH)_x$ under pressure by Moses *et al.*[87] yielded somewhat higher values, namely $E_{\rm gap}^{\rm 1D}=1.7$–1.8 eV and the minimum 3D gap $E_{\rm gap}=1.45\pm0.05$ eV. These values are in good agreement with other optical data,[91,92] including recent measurements in highly oriented, nonfibrous Durham-Graz material, which indicate an intrinsic band gap of crystalline *trans*-$(CH)_x$ around 1.5 eV.[90,93] Still, a precise experimental determination of the actual intrinsic principal gap in crystalline *trans*-$(CH)_x$ is hampered by the inadvertent defects and broken chains in the material which make it difficult to assign the observed broadening and the band-edge tail in the absorption spectrum unambiguously to interchain coupling or to defects.

In Fig. 18 we have compared the joint density of states from our LDA calculation of *trans*-$(CH)_x$ in the $P2_1/a$ structure with the recent experimental absorption data in Durham-Graz *trans*-$(CH)_x$.[53,93] In view of the uncertainty caused by $\Sigma_{\rm el}$ we have positioned the two curves so that their peaks coincide. This requires taking a self-energy of $\Sigma_{\rm el}=0.74$ eV, which is consistent with that chosen in Figs. 12 and 16. This procedure therefore al-

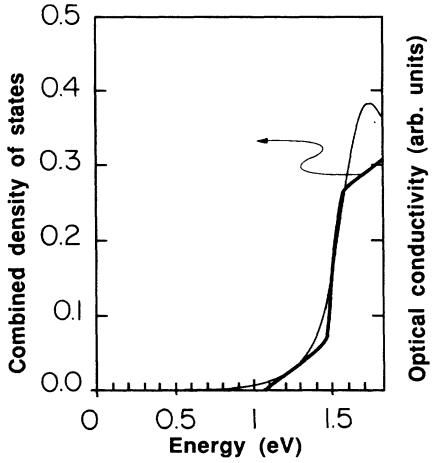

FIG. 18. A comparison of the experimental optical absorption (Ref. 93) of Durham-Graz *trans*-$(CH)_x$ (thin line) with the joint density of states predicted by the LDA calculation of *trans*-$(CH)_x$ in the $P2_1/a$ structure (thick line). The "one-dimensional" peaks have been chosen to coincide.

lows a determination of the intrinsic minimum energy gap of crystalline 3D *trans*-polyacetylene; from Fig. 18 we deduce a value of 1.1 eV. The experimental band-edge data show a tail which is somewhat more extended than the LDA results; this is due in part to the effects of defects and imperfections not included in the theory.

Recent results using LDA–band-structure calculations based on linear muffin-tin orbitals[94,95] have suggested a substantial difference in the optical absorptions expected for the $P2_1/a$ and $P2_1/n$ structures in *trans*-$(CH)_x$. Our data on the joint densities of states in the two structures do not support this expectation; we are currently working on a full calculation of the optical absorption using our results and hope to return to this point in a future publication.

III. INTRINSIC DEFECTS: SOLITONS, POLARONS, AND BIPOLARONS

Charge carriers in strictly one-dimensional deformable systems will always self-trap (in the adiabatic approximation) due to the electron-phonon interaction. The self-trapped charge and the accompanying atomic displacement pattern form a polaron. In three dimensions, on the other hand, the electron-phonon interaction is able to localize charge carriers only in the limit of strong coupling, which is not thought to be relevant for polyacetylene. Thus in general, carriers in intrinsically 3D materials remain delocalized. Emin[36] has given an excellent discussion of this general behavior, as well as of exceptions, in a wide range of materials. Intuitively, the situation is analogous to a particle in an attractive well. In one dimension, there is a bound state for any well depth, whereas in three dimensions, a localized state occurs only when the potential strength exceeds a certain threshold value.

Given our conclusion that the states near the band edge in crystalline *trans*-$(CH)_x$ exhibit splittings due to interchain couplings, it is natural to ask whether this interchain interaction is sufficiently strong to render the material intrinsically three-dimensional and hence unlikely to support polarons (as has recently been claimed by Emin[23]) or whether charge carriers self-trap, as predicted by most of the (primarily 1D) theoretical models studied thus far.

To study the influence of the interchain interaction on intrinsic defects in 3D crystalline *trans*-$(CH)_x$, we consider frozen-in displacement patterns of the ions corresponding to "polaronlike" and "bipolaronlike" configurations. We then investigate the electronic structure corresponding to these configurations to see whether there are any *intra*gap electronic "bound" states. If there are no such states and all electronic states are *de*localized, then we can conclude that there are no localized, self-trapped intrinsic defects and that the 3D couplings have destabilized the nonlinear excitations characteristic of 1D systems.

To avoid possible confusion about the interpretation of our results, we should define these configurations more precisely. In the 1D continuum version of the SSH model, the displacement $\Delta(x)$ associated with a polaron is shown schematically in Fig. 19(a). This figure also shows schematically the "single-site" polaronlike configuration which we shall later introduce. In Fig. 20, the bipolaronlike displacement pattern is shown; in terms of the continuum model, this displacement corresponds to a very weakly bound kink-antikink pair, the "separation" of which is called d_{BP} in the figure.

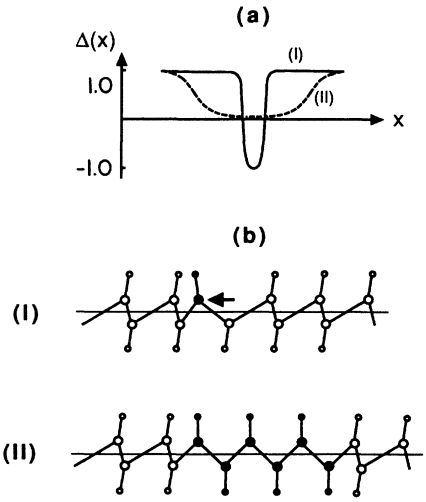

FIG. 19. Schematic atomic displacement patterns corresponding to the "polaronlike" defect discussed in the text: (a) sketches of the "continuum limit" order parameter for the case of the (strongly distorted) single-site polaron (solid curve, labeled I) and extended polaron (dashed curve, labeled II); (b) the atomic positions (with the dimerization amplitude greatly exaggerated for clarity) corresponding to (I) a localized, "single-site" polaron and (II) an extended polaron.

In the 1D model, the two distortions extend over approximately 15 C—H units; this is more than we can accurately take into account in our full 3D electronic-

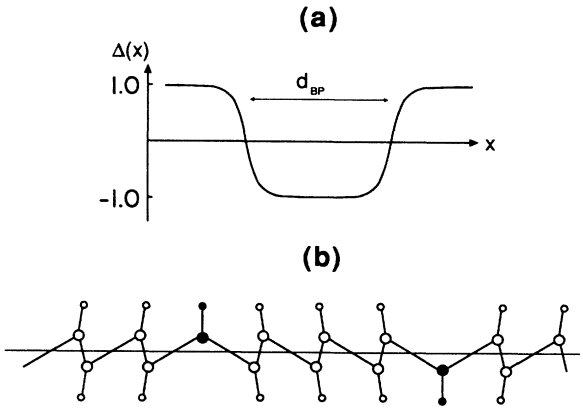

FIG. 20. Schematic atomic displacement pattern corresponding to the "bipolaronlike" defect discussed in the text: (a) a sketch of the "continuum limit" order parameter for the bipolaron, showing the effective separation d_{BP} of the kink and antikink; (b) the atomic positions (with the dimerization amplitude greatly exaggerated for clarity) corresponding to a bipolaron, i.e., a pair of confined kink-antikink solitons.

structure calculations. In our actual calculations, therefore, we consider primarily the two limiting cases shown in Figs. 19 and 20: (1) the polaronlike distortion, in either its single-site variant [Figs. 19(a) and 19(b), curve I] or with an extended region of partial bond-order reversal [Figs. 19(a) and 19(b), curve II], and (2) a bipolaronlike distortion corresponding to a complete bond-order reversal extending over a range between 1 and 6 C—H units (Fig. 20). Since both these distortions are nontopological, the major difference between a "polaron" and a "bipolaron" in our study is the complete bond-order reversal between kink and antikink in the bipolaron in contrast to a partial bond-order reversal for the polaron. We then vary the degree of bond alternation in all of these defects and study the induced bound states in the gap.

In the limit of infinite displacement $\Delta(0)=\infty$, the approximate particle-hole symmetry guarantees that even the single-site "polaronlike" defect (Fig. 19, curve I) must eventually develop two bound states close to midgap, since such a displacement simply corresponds to breaking the bonds. Similarly, a bipolaronic displacement with complete bond-order reversal—such as depicted in Fig. 20—will also lead to near-midgap levels in the limit of infinite separation of the kink and antikink, since this situation represents two separated solitons. These limiting cases are not relevant to real defects, of course.

A. The Koster-Slater approach to defect calculations

To examine a spatially localized defect in an otherwise perfect crystal with translational invariance it is most convenient to use the scattering-theoretic Green-function technique.[54] In this method, the spectrum of the perturbed Hamiltonian $H=H_0+v$ is calculated by solving the perturbed Schrödinger equation in the form

$$|\psi\rangle=(E-H_0)^{-1}V|\psi\rangle=G_0(E)V|\psi\rangle \ . \tag{3.1}$$

Here, H_0 is the unperturbed Hamiltonian and $G_0(E)$ is the Green function of the perfect crystal. The bound states E_T in the gap are then obtained from the zeros of the determinantal equation

$$\det[1-G_0(E_T)V]=0 \ . \tag{3.2}$$

The size of this matrix equation is determined by the range of the defect potential V.

1. The perfect-crystal Hamiltonian

A fully self-consistent density-functional calculation of an extended defect in a crystal with only monoclinic symmetry is at present not feasible, even with modern supercomputers. Therefore, we have mapped the first-principles calculations for the perfect *trans*-$(CH)_x$ crystal onto an accurate, multi-orbital, three-dimensional tight-binding model. Although empirical, this approach is, we believe, quite accurate; indeed, it has recently been demonstrated that the electronic structure of a wide variety of solids can be successfully predicted with semiempirical tight-binding models containing only universal Hamiltonian matrix elements.[96,97] Following these ideas, we have determined the matrix elements by initializing the fitting procedure with the universal tight-binding parameters of Ref. 97. Subsequently, these parameters have been fine tuned to obtain quantitative agreement with our first-principles local-density calculations. It turns out that a nearest-neighbor tight-binding model with a single s state and three p states per site, plus the interactions between the H and the adjacent C atoms on neighboring chains (as indicated by the dashed lines in Figs. 2 and 3), can account *quantitatively* for all of the following electronic structure properties, as calculated by the LDA: (i) the electronic band structure in the gap region; (ii) the atomic character of the bands as obtained from integrated charge densities in each valence band; and (iii) the deformation potentials, i.e., the changes of the band-edge states upon dimerization, throughout the Brillouin zone. We find it essential, however, to include all two-center interaction matrix elements allowed by symmetry. The basis states can be labeled by the site I and the angular momentum quantum numbers l and m. The z component of the angular momentum m is defined

TABLE IV. Tight-binding parameters for three-dimensional *trans*-$(CH)_x$. The first column (on-site) gives the on-site Hamiltonian matrix elements, the other columns give the intersite parameters η and d_0, defined in Eq. (3.3), for nearest-neighbor pairs of atoms, both on the same chain and on adjacent chains in the unit cell.

	On site	C-C intrachain	C-H intrachain	C-H interchain
$\varepsilon_{s,H}$ (eV)	−13.61			
$\varepsilon_{s,C}$ (eV)	−16.0			
$\varepsilon_{p,H}$ (eV)	0.0			
$\varepsilon_{p,C}$ (eV)	−11.79			
d_0 (Å)		0.8583	0.6945	1.8198
$\eta_{ss\sigma}$		−1.81	−1.81	−0.65
$\eta_{sp\sigma}$		1.30	1.22	1.32
$\eta_{pp\sigma}$		1.76	1.44	1.34
$\eta_{pp\pi}$		−0.55	−0.72	−0.39

with respect to the axis connecting the atomic sites. The intersite Hamiltonian matrix elements are fitted to the following functional form:

$$t_{III'l'm}=\frac{\hbar^2}{m_e d_0^2}\eta_{ll'm}^{II'}e^{-2(d-d_0)/d_0}\ , \tag{3.3}$$

where m_e is the electron mass and d is the distance between the atoms. The constants d_0 and $\eta_{ll'm}$ and the diagonal Hamiltonian matrix elements ε_{Il} are given in Table IV. For $d_0=d$, the matrix elements follow Harrison's d^{-2} scaling rule;[96] the parameter d_0 has been introduced to provide an accurate fit to the deformation potentials.

Since the tight-binding parameters reproduce the local-density-functional calculations accurately, they also underestimate the principal energy gap. The calculated minimum energy gap is 0.40 eV in the $P2_1/a$ structure; note that this implies a "1D" LDA gap of approximately 0.76 eV (see the discussion in Sec. II C 7). Since we wish to calculate impurity binding energies, this would seem to introduce an appreciable uncertainty in the level energies in the gap. Actually, however, the local-density formalism has been shown to predict impurity level energies in excellent agreement with experiment, *provided* the level energies are calculated with respect to the band edge they are primarily derived from.[98] In the present case, the situation is particularly favorable in this respect since we are predominantly interested in the threshold defect potential which leads to the formation of a bound state. This threshold is controlled by the density of states at the band edge and not by the gap.

In Fig. 21(a) we show the calculated tight-binding band structure for the $P2_1/a$ structure of *trans*-polyacetylene. The lower energy bands differ somewhat from the LDA bands, shown in Fig. 21(b) for comparison, but all major features of the bands near the Fermi energy which are relevant for the defect calculations discussed below are accurately reproduced.

The tight-binding calculation reveals that the splittings of the band-edge states near the $\mathbf{k}$ point $\mathbf{k}_B$, which we discussed in detail in Sec. II C, are predominantly caused by the $t_{p,\mathrm{C};p,\mathrm{H};\sigma}$ interchain matrix element; the contribution of the $t_{p,\mathrm{C};s,\mathrm{H};\sigma}$ matrix element to the band edge states is zero by symmetry. This geometrical fact that the interchain coupling is mediated by a particular carbon-hydrogen overlap has especially important consequences for comparisons with previous theoretical attempts to take interchain couplings into account within a tight-binding approximation. In particular, simple "two-chain" models[6,35,38–40] cannot fit our full 3D tight-binding band structure, since the geometrical structure dictated by the manner in which the hydrogen and carbon orbitals overlap causes adjacent carbons on a given chain to interact effectively with *different* chains in the unit cell. Thus although one can concoct a straightforward tight-binding scheme with a single effective interchain coupling, it does not reduce to a two-chain model. We intend to return to this point in a future publication.

It is instructive to consider the limiting case of a SSH-type model where only the nearest-neighbor intrachain $t_{p,\mathrm{C};p,\mathrm{C},\pi}$ matrix elements are taken into account explicitly in the energy bands. With the parameters given in Table IV and Eq. (3.3), one finds

$$t_{p,\mathrm{C};p,\mathrm{C};\pi,\ \mathrm{intrachain}}=t_0\pm\alpha u_{\mathrm{C}}\ \mathrm{eV} \tag{3.4}$$

with $t_0=-2.20$ eV and $\alpha=4.52$ eV Å^{-1}. In Eq. (3.4), the two signs correspond to the alternating bond lengths and u_{C} is the dimerization (see Table II). The values for t_0 and α are similar to widely used Hückel parameters in *trans*-polyacetylene.[99]

Having determined the perfect crystal Hamiltonian H^0 with Bloch states $\psi_{n\mathbf{k}}$ in a localized basis $|I\lambda\rangle$, where I denotes the atomic site and λ the orbital symmetry of the basis state, we can now compute the Green function G^0 in this basis,

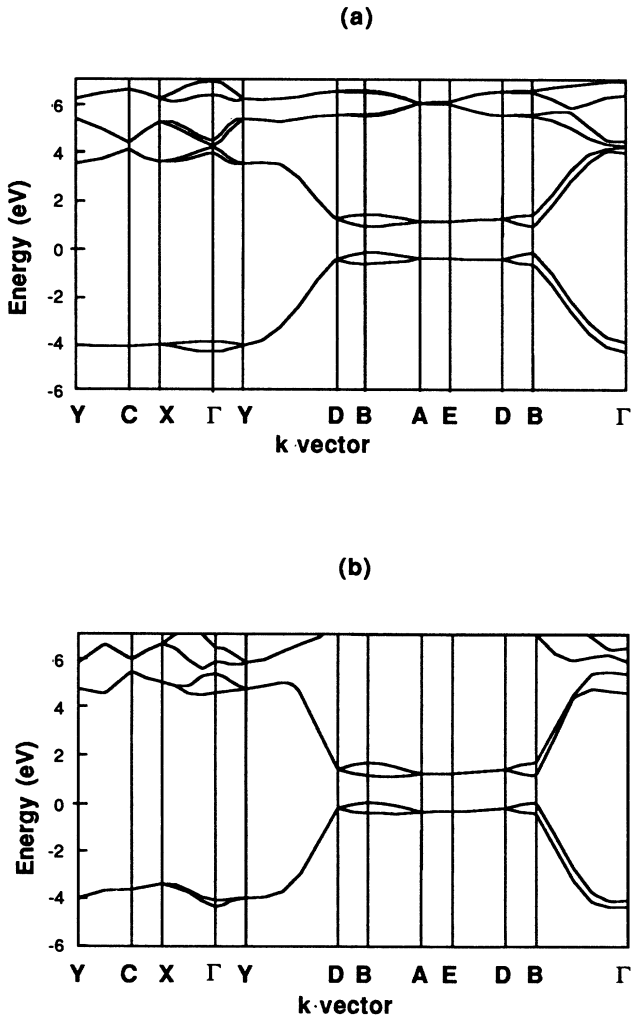

FIG. 21. Comparison of calculated electronic band structures within the density-functional approach (a) and the multi-orbital tight-binding model used to compute the electronic structure of the intrinsic defects (b). The similarity of the bands close to the minimal energy gap gives credence to the tight-binding calculations.

$$G^0_{I\lambda,I'\lambda'}(E)=\int dE' \frac{D_{I\lambda,I'\lambda'}(E')}{E-E'} , \tag{3.5}$$

$$D_{I\lambda,I'\lambda'}(E)=\sum_{n,\mathbf{k}} \langle I\lambda|\psi_{n\mathbf{k}}\rangle\langle\psi_{n\mathbf{k}}|I'\lambda'\rangle\delta(E-E_{n\mathbf{k}}) . \tag{3.6}$$

The Brillouin-zone integration in Eq. (3.6) was performed by using an improved version of the tetrahedron method of Lehmann and Taut[100] and including 4851 **k** points in the irreducible wedge. Since there are eight atoms per unit cell and four basis states per atom, G^0 represents a 32×32 matrix. Correspondingly, there are 32 bands to be summed over in Eq. (3.6); it turns out that the results for the defect states change only insignificantly if this sum over the band index n is restricted to four bands below and four above the Fermi energy.

2. *The defect matrix*

The defect matrix can be expressed in terms of the orthogonal, localized tight-binding basis functions $|I\lambda\rangle$, defined in Sec. III A 1, as

$$V_{I\lambda,I'\lambda'}=\langle I\lambda|H|I'\lambda'\rangle-\langle I\lambda|H^0|I'\lambda'\rangle . \tag{3.7}$$

With Eq. (3.3), the intersite Hamiltonian matrix elements in Eq. (3.7) are known explicitly as a function of the distance between the atomic sites. We assume that the (on-site) diagonal Hamiltonian matrix elements and the parameters η and d_0 do not change upon lattice distortions. This approximation accurately reproduces the bulk deformation potentials calculated in the framework of the density-functional method and has also been employed and tested extensively in previous work on defects in semiconductors.[101]

For any given lattice distortion on a single C—H chain, the defect matrix can be calculated from Eq. (3.7), using Eq. (3.3). When we freeze in a lattice distortion on one chain, the interchain interaction causes the defect matrix to be nonzero on the distorted chain as well as on the neighboring chains. With the Green function from Eqs. (3.5) and (3.6), the eigenstates and energies of the perturbed crystal, Eqs. (3.1) and (3.2), can be computed.

B. Polaronlike defects

In our calculation of "polaronlike" configurations, we shall use the distortions shown schematically in Figs. 19(b). Note that in all cases, we shall assume that the distortions occur on a single chain and are embedded in an otherwise perfect three-dimensional crystal. In single *trans*-$(CH)_x$ chains, theoretical studies based on the SSH model predict that a polaron is the lowest energy state available to a singel added electron (or hole).[102–104]

Let us start with the single-site polaronlike distortion [Fig. 19(b), curve I]. Recent calculations show[105] that the bound states in the energy gap produced by such a "single-site" defect are only slightly shallower than those produced by an extended defect. Thus by increasing the distortion in the former defect, we can simulate a spatially more extended lattice distortion. In Fig. 22, we have plotted the bound states in the energy gap as a function of the displacement of the single-site polaron. The

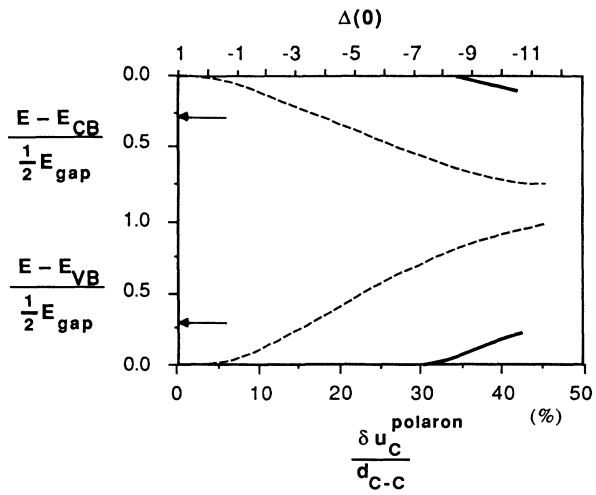

FIG. 22. The intragap electronic levels E as a function of distortion for a "single-site" polaron, as depicted in Fig. 19(b), curve I. The solid curve is with the actual interchain coupling predicted by our calculations; the dashed curve is the idealized purely 1D result. The arrows indicate the position of the bound polaron states in a continuum SSH-type 1D model. The distortion is given relative to the nearest-neighbor distance $d_{C\text{-}C}$ and in terms of the dimensionless distortion parameter Δ at the polaron center, as depicted in Figs. 19(a), curve I and 19(b), curve I. The bound states E are plotted relative to band edge they are primarily derived from.

dashed lines are single-chain calculations, where all interchain matrix elements are set equal to zero, while the full three-dimensional calculations indicated by solid lines, are obtained from the complete 3D calculation. The position of the polaron bound state energies in simple 1D continuum model are also shown (indicated by arrows). As one can deduce from this figure, a 15% distortion δu_C leads to bound state energies close to those of the continuum model, *provided* we turn off all interchain couplings. Once the interchain coupling is included, however, *no bound states appear in the energy gap* up to distortions exceeding 35% of the bond length, which are physically unattainable.

As a second model for a polaron, we consider an extended distortion of the type shown in Fig. 19(b), curve II. Here we vary the degree of bond alternation between the perfectly dimerized situation [$\Delta(0)=1$] and n completely undimerized C—H units [$\Delta(0)=0$] with $n=6$. The result is shown in Fig. 23. Only the case of no interchain coupling is shown since no trap states are formed with the realistic interchain interactions included. As in the previous case, we thus find the interchain interaction completely suppresses the formation of bound states in the gap.

The numerical results in Fig. 22 were obtained with an equilibrium value of $u_C=0.05$ Å and the $P2_1/a$ structure. We find that smaller dimerizations do not visibly deepen the bound states, because a shallow bound state is generated primarily from electronic states very close to the band edge. Consequently, its formation is insensitive to the gap itself, and therefore, to the dimerization. We

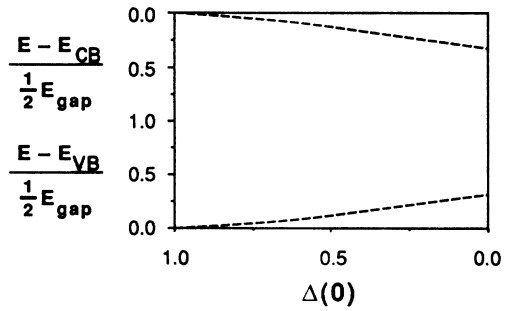

FIG. 23. The intragap electronic levels as a function of the distortion shown schematically in Fig. 19(b), curve II, which models a more extended polaron. In the calculations, the defect has been chosen to extend over 6 $(CH)_2$ units [rather than 3, as indicated in the schematic Fig. 19(b), curve II]. With the actual interchain coupling included, no bound states are formed in the gap. The dashed lines are the idealized purely 1D result.

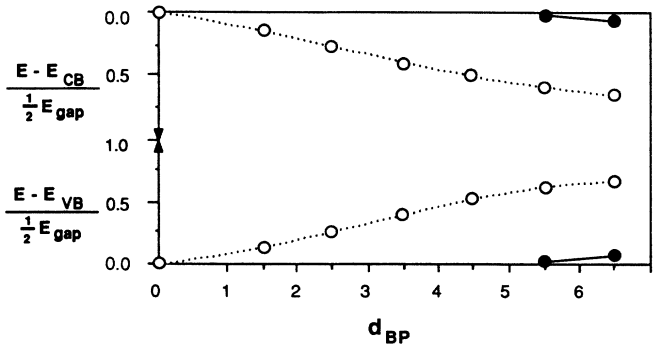

FIG. 24. The intragap electronic levels as a function of separation d_{BP}, for a bipolaronlike defect described in Fig. 20. The corresponding distortion is depicted in Fig. 20(b). The solid circles are with interchain coupling; the open circles are the purely 1D result. The connecting lines are drawn only to guide the eye. In our calculations, the distorted chain is embedded in the 3D crystal.

have also performed the Green-function calculations in the $P2_1/n$ structure. Since the band-edge splittings and, correspondingly, the interchain interactions are smaller in this structure (see Fig. 13) and it is also easier to form bound states in the energy gap. We find, however, that to obtain a bound state still requires a (physically unlikely) distortion of 20%.

Our calculations also show that a distortion of the hydrogen atom with respect to its adjacent carbon atom has only a negligible effect on the bound states. The major effect of the interchain interaction is contained in the perfect crystal's Green function and not in the interchain part of the defect matrix.

Thus our LDA results suggest that the three-dimensional character of the band-edge states prevents the formation of intragap electronic states and consequently of self-trapped polarons in crystalline *trans*-polyacetylene. Bound states in the energy gap can be formed in principle but to do so requires unrealistically large lattice distortions of the C—C distance. The energies associated with these large displacements cannot be compensated by a corresponding gain in electronic energy. As a consequence, an extra electron which is placed into the conduction band will remain a free carrier with an effective mass $m^* \approx m_e$.

C. Bipolaronlike defects and kink solitons

SSH-type calculations in single chain models of *trans*-$(CH)_x$ predict that photoexcited electron-hole pairs form bipolarons which rapidly decay into separated kink and antikink solitons.[106,107] In Fig. 20 we depict the displacement pattern corresponding to separated kink and antikink solitons. The distance between the two undimerized C—H pairs in this figure is 2.5 lattice constants along the c axis. We have performed three-dimensional Green-function calculations with frozen-in "bipolaronlike" distortions having various separations d_{BP} on a single chain in otherwise perfect crystalline *trans*-$(CH)_x$ in the $P2_1/a$ structure. The results for the binding energies as a function of d_{BP} are summarized in Fig. 24. As in Fig. 22, the dashed lines show the results with all interchain matrix elements set equal to zero, while the full lines represent the defect levels in the three-dimensional crystal.

As in the case of the polaron, interchain coupling strongly impedes the formation of bound states in the energy gap of three-dimensional *trans*-$(CH)_x$. Only for separations exceeding 6 lattice constants (12 carbon sites in chain direction) between the kink and antikink soliton on one chain does a pair of shallow bound states appear in the energy gap. For larger separations, two bound states remain in the gap and, in the limit of infinite kink-antikink separation, lie close to the gap center. Due to the mixing of carbon and hydrogen wave functions and the consequent breaking of particle-hole symmetry, they do not lie exactly in the center of the gap even in the limit of infinite separation. For more realistic separations, the bound states are quite shallow; by extrapolating our results we estimate the binding energies barely exceed room temperature thermal energies for distances smaller than 8–10 lattice constants, for example.

Although bipolaron lattice configurations do produce intragap electronic bound states, the stability of genuine bipolarons requires more. First, one must analyze the overall energetics of bipolaron formation. Apart from the energy to distort the particular chain on which the bipolaron resides, the formation of a separated kink-antikink pair costs interchain bonding energy, since the dimerization in between the kinks is out of phase with the dimerizations on the adjacent chains. We estimate from our total energy calculations that the maximum kink separation attainable in a perfectly ordered crystal is of the order of 50 lattice constants in chain direction. Since the electronic wave function in a kink-bound state is expected to extend over 5–10 lattice constants,[17] this interchain confinement to 50 lattice constants strongly limits the formation of a bipolaron. In the $P2_1/a$ structure, it is probably less than that due to the stronger interchain coupling. Second, if two electrons are localized in the bipolaronic intragap levels, Coulomb repulsion effects will

further reduce the total effective binding energy and hence tend to destabilize the bipolaron.

Although these results do not entirely preclude the possibility of formation of bipolarons in perfect crystalline *trans*-$(CH)_x$, they do call into question previous discussions of the energetics of these nonlinear excitations. In particular, our results appear to make it more likely that thermal fluctuations or direct Coulomb repulsion between the two electrons in the bipolaron can destabilize this localized intrinsic defect even if it is formed.

IV. DISCUSSION AD CONCLUSIONS

In the discussion of our results, it is appropriate to begin with several general comments concerning the local-density-functional (LDA) approach. Although ideally one would want to include realistic geometry, chemical structure, and all electron correlation effects in a full three-dimensional calculation of large molecules or crystalline solids, such calculations are—and will remain for the foreseeable future—simply impossible to carry out. Thus one is compelled to adopt approximate procedures such as the LDA. Of course, this method does not treat correctly all effects of electron correlations. Nonetheless, it represents an essential first step in understanding the full three-dimensional structure of molecules and crystalline solids.

Within the LDA, we believe that our results for *trans*-$(CH)_x$ represent the most accurate calculations to date, going considerably beyond previous results in accuracy, completeness, convergence, and internal consistency. For instance, the computation of the Hellmann-Feynman forces on the ions proved crucial for a proper assessment of the broken-symmetry ground state predicted by LDA. This is in contrast to earlier calculations[42] which—for technical reasons—were unable to evaluate the Hellmann-Feynman forces. Thus we feel that our results accurately reflect the true predictions of the LDA approach for perfect crystalline *trans*-$(CH)_x$.

Our three-dimensional LDA calculation is in a sense complementary to the many recent detailed one-dimensional studies of the effects of correlations in conducting polymers. Dimersionality, like correlations, can have a profound effect on the properties of real materials. We believe that our LDA results, although by no means definitive, strongly suggest that the effect of three dimensionality is essential to understanding the behavior of crystalline *trans*-$(CH)_x$.

Apart from the general issue of the applicability of LDA, the small energy difference that we calculate between the $P2_1/a$ and $P2_1/n$ structures is a natural cause for concern, since it is indeed tiny by LDA or *ab initio* chemical standards. However, here one should recall several points. First, based on our detailed convergence studies, we are confident that our results represent the correct solution to the LDA equations and that the energy difference we calculate (0.01 eV) is outside our numerical error (± 0.003 eV). Second, while the difference of 0.01 eV per unit cell is quite small, it is important to remember that the two structures are in fact *very* similar. In this regard it should also be noted that in semiconductors, structural energy differences corresponding to phonons with an energy of significantly less than 0.01 eV are predicted with high accuracy by the LDA, even though the total cohesive energy itself is predicted with a substantially large error.[108] Third, as far as we can test the trends of the energy difference with respect to various perturbations, they are in accord with physical expectations based on the structures. Decreasing the dimerization, for example, brings the overlapping hydrogen and carbon orbitals on adjacent chains into closer alignment, thereby increasing the energy difference between the two structures. Thus, although the energy difference is only 0.01 eV for the experimental value of the dimerization (0.05 Å), for the force-free dimerization (0.01 Å) this difference is 0.03 eV. A second, separate correct trend is the decrease in energy difference when the distance between the chains in the unit cell is artificially increased. Fourth and finally, even if one accepts that due to correlation effects not correctly modeled by the LDA calculation the relative placement of the $P2_1/a$ and $P2_1/n$ structures could be changed, one should note that in both cases the states near the band edge contain strong three-dimensional contributions; thus our further considerations regarding the possible importance of three-dimensional structure for intrinsic defects will remain qualitatively unchanged, independent of which of the two structures is the true ground state.

Regarding the separate but vital issue of whether the LDA approach correctly captures the properties of the real material, two pieces of indirect evidence seem to us to make plausible the assertion that the LDA predictions may be accurate for the ground state of the crystalline *trans*-$(CH)_x$. First, in solid Xe, the LDA predicts not only the equilibrium lattice constant quantitatively but also the transition (under pressure) from the insulating to the metallic phase.[63] Second, in finite polyenes, the primary motivation for studying correlation effects came from the observed behavior of the excited states, both optically allowed and forbidden. Independent-electron theories seem adequate for treating the ground state properties—e.g., energies of various ionic geometries of these systems.[9] These two results suggest that in *trans*-$(CH)_x$ neither weak interchain coupling nor the polymeric nature of the material represents an in-principle impediment to an LDA calculation. In addition, although it is always possible that the LDA results we obtain are correct for the wrong reasons, we feel that it is important to stress that recent refined experimental analyses strongly suggest that the true structure of crystalline *trans*-$(CH)_x$ is indeed $P2_1/a$ (see Sec. II B).[34,53] It seems also appropriate to point out that recent progress in studies of the "self-interaction-corrected"[82,109] (SIC) LDA suggests that the near-term prospects for obtaining a deeper understanding of the limitations of LDA—and, possibly, for a systematic method for removing these limitations—are improving.

A third broad issue raised by our results concerns the nature and stability of intrinsic defects in three-dimensional crystalline *trans*-$(CH)_x$. Without recapitulating the full discussion of Sec. III, we recall that we expect polarons to be destabilized by three-dimensionality

effects whereas bipolarons may remain stable, although much less robust that the one-dimensional models would suggest. We feel that these results must be accepted as the best presently available calculations of defects in the true three-dimensional perfect crystal. In particular, our tight-binding fit accurately reproduces the results of the full LDA calculation, including realistic geometry, multi-orbital band structure, and electron-phonon coupling constants. Further, we obtain quantitative estimates for the behavior of intragap levels which, when we artificially turn off the interchain coupling, correctly reproduce the earlier one-dimensional results. Second, our results on the destabilization of the "polaron" distortion are not sensitive to our conclusions on the ground-state structure in the sense that for physically plausible lattice distortions we find no bound states in the gap in either the $P2_1/n$ or $P2_1/a$ structures. Third, the failure of the LDA to obtain the correct dimerization and gap is not expected to invalidate the estimate of the threshold polaronic displacement required to form a bound state in the gap, as discussed in Sec. III A. Fourth, previous studies of electron-electron interaction effects in one-dimensional models of $(CH)_x$ and related conjugated polymers as well as substantial literature on Coulomb effects in conventional semiconductors suggest that for localized intrinsic defects—including solitons, polarons, and bipolarons—Coulomb effects typically drive the intragap levels associated with localized defects away from the center of the gap toward the band edges, thereby reducing the depth of the bound states. Thus, we believe, that the correct inclusion of Coulomb effects would further destabilize these localized excitations.

Finally, we come to the essential issue of the applicability of our results to presently existing conducting polymers. Here we should reemphasize that our calculations have been carried out for perfectly ordered crystalline, three-dimensional *trans*-$(CH)_x$. At present, the chain lengths even in highly oriented, crystalline Graz-Durham *trans*-$(CH)_x$ are smaller than 40 C—H units[34,51] and there is a high density of broken bonds. In the morphologically complex Shirakawa material, many chains are in a highly disordered environment near the fibril surface;[110,111] it is thus conceivable that observables such as optical excitations in this material exhibit properties which are more characteristic of single chains of *trans*-$(CH)_x$ than of a three-dimensionally ordered crystal.

On the other hand, one must recognize that the possible roles of the nonlinear excitations predicted by the 1D theories in describing, for example, the transport, optical absorption, and photoexcited states in *trans*-$(CH)_x$ has remained controversial (see, e.g., Refs. 2, 3, 99, 112, and 113 for critical reviews of conflicting data). In particular, although much optical absorption data have been interpreted in terms of kink-antikink or bipolaron excitations, even the most recent fast photoinduced absorption experiments have still failed to produce direct experimental evidence for polarons.[114] Many experimental observations in *trans*-$(CH)_x$ may be interpretable in terms of spatially fixed defects[112] or dynamic rearrangements of defect states[115] which are not unique to one-dimensional systems. From studies of deep traps and dangling bonds in semiconductors and ionic crystals, it is well established that disorder tends to produce states in the gap. Indeed, given the relatively low "purity" of the current *trans*-$(CH)_x$ crystals, with their large number of extrinsic defects and impurities, broken bonds, and sp^3 cross links, it is likely that many of the observed intragap states are, in fact, of extrinsic origin. For instance, it has been shown theoretically that several immobile defects in *trans*-$(CH)_x$ have the same spin-charge relation as kink solitons and tend to produce mid-gap levels.[105,116,117] Further, the possible nonsolitonic and extrinsic nature of the picosecond photoconductivity in *trans*-$(CH)_x$ has recently been suggested.[118]

The ultimate explanation of the various physical phenomena associated with the intragap levels observed in real samples of *trans*-$(CH)_x$ will require considerable further study and is obviously beyond the scope of any single article. We hope, however, that our present state-of-the-art LDA calculation represents an essential foundation for these further investigations and that extensions of the technique to determinations of optical absorption[94,95] will help to provide further insights into these exciting novel materials.

ACKNOWLEDGMENTS

We are grateful to Dionys Baeriswyl, Richard Friend, Günther Leising, and Otto Sankey for many enlightening discussions. We thank the Center for Materials Science and Center for Nonlinear Studies for computational support at Los Alamos National Laboratory and the Computational Sciences Division of the U.S. Department of Energy (DOE) for computational support at the National Magnetic Fusion Energy Computing Center at Lawrence Livermore National Laboratory. One of us (P.V.) is grateful to the Max Kade Foundation for support of his visit to Los Alamos, where this work was begun. The other (D.C.) thanks the Institut für Theoretische Physik of the Karl-Franzens-Universität in Graz for its hospitality during the completion of the work. This work was supported by the Jubiläumsfonds der Österreichischen Nationalbank, and by the U.S. DOE.

*Permanent address: Institut für Theoretische Physik, Universität Graz, Universitätplatz 5, A-8010 Graz, Austria.

[1]For the most recent in the series of conference proceedings reviewing all aspects of this and related issues, see Synth. Met. **27** (1988); **28** (1989); **29** (1989).

[2]A. J. Heeger, S. Kivelson, J. R. Schrieffer, and W.-P. Su, Rev. Mod. Phys. **60**, 781 (1988).

[3]D. Baeriswyl, D. K. Campbell, and S. Mazumdar, in *Conducting Polymers,* edited by H. Kiess (Springer, Heidelberg, in press).

[4]Lu Yu, *Solitons and Polarons in Conducting Polymers* (World Scientific, Singapore, 1988).

[5]A. A. Ovchinnikov and I. I. Ukrainskii, Sov. Sci. Rev. B: Chem. **9**, 125 (1987).
[6]S. A. Brazovskii and N. N. Kirova, Sov. Sci. Rev. A: Phys. **5**, 100 (1984).
[7]W. Hückel, J. Phys. **70**, 204 (1931); **76**, 628 (1932).
[8]L. Salem, *Molecular Orbital Theory of Conjgated Systems* (Benjamin, London, 1966).
[9]B. S. Hudson, B. B. Kohler, and K. Schulten, in *Excited States,* edited by E. C. Lin (Academic, New York, 1982), p. 1.
[10]M. F. Granville, G. R. Holtom, and B. E. Kohler, J. Chem. Phys. **72**, 4671 (1980).
[11]R. Pariser and R. G. Parr, J. Chem. Phys. **21**, 767 (1953); J. A. Pople, Trans. Faraday Soc. **42**, 1375 (1953).
[12]Z. G. Soos and S. Ramasesha, Phys. Rev. Lett. **51**, 2374 (1983).
[13]S. Ramasesha and Z. G. Soos, J. Chem. Phys. **80**, 3278 (1984).
[14]H. Thomann, L. R. Dalton, M. Grabowski, and T. C. Clarke, Phys. Rev. B **31**, 3141 (1985).
[15]M. Mehring, A. Grupp, P. Höfer, and H. Käss, Synth. Met. **28**, D399 (1989).
[16]A. A. Ovchinnikov, L. I. Ukrainskii, and G. V. Kventsel, Usp. Fiz. Nauk **108**, 81 (1972) [Sov. Phys.—Usp. **15**, 575 (1973)].
[17]W.-P. Su, J. R. Schrieffer, and A. J. Heeger, Phys. Rev. Lett. **42**, 1698 (1979); Phys. Rev. B **22**, 2099 (1980); **28**, 1138(E) (1983); **29**, 2309 (1984).
[18]C. R. Fincher, C.-E. Chen, A. J. Heeger, A. G. MacDiarmid, and J. B. Hastings, Phys. Rev. Lett. **48**, 100 (1982).
[19]C. W. Yannoni and T. C. Clarke, Phys. Rev. Lett. **51**, 1191 (1983).
[20]J. P. Pouget, P. Robin, R. Comes, M. W. Gibson, A. J. Epstein, and D. Billaud, Physica B+C (Amsterdam) **127B**, 158 (1984).
[21]J. P. Pouget, in *Electronic Properties of Polymers and Related Compounds,* Vol. 63 of *Springer Series in Solid State Sciences,* edited by H. Kuzmány, M. Mehring, and S. Roth (Springer, Heidelberg, 1986), p. 26.
[22]S. A. Brazovskii, L. P. Gor'kov, and J. R. Schrieffer, Phys. Scr. **25**, 423 (1982).
[23]D. Emin, Phys. Rev. B **33**, 3973 (1986).
[24]R. H. Baughman, S. L. Hsu, G. P. Pez, and A. J. Signorelli, J. Chem. Phys. **68**, 5405 (1978).
[25]R. H. Baughman and S. L. Hsu, J. Polym. Sci. **17**, 185 (1979).
[26]R. H. Baughman, S. L. Hsu, L. R. Anderson, G. P. Pez, and A. J. Signorelli, in *Molecular Metals,* edited by W. E. Hatfield (Plenum, New York, 1979), p. 87.
[27]R. H. Baughman and G. Moss, J. Chem. Phys. **77**, 6321 (1982).
[28]P. M. Grant and I. P. Batra, Solid State Commun. **29**, 225 (1979).
[29]P. M. Grant and I. P. Batra, Synth. Met. **1**, 192 (1979/1980).
[30]P. M. Grant and I. P. Batra, J. Phys. (Paris) Colloq. **44**, C3-437 (1983).
[31]J. Ashkenazi, E. Ehrenfreund, Z. Vardeny, and O. Brafman, Mol. Cryst. Liq. Cryst. **117**, 193 (1985).
[32]J. Ashkenazi, W. B. Pickett, B. M. Klein, H. Krakauer, and C. S. Wang, Bull. Am. Phys. Soc. **32**, 929 (1987).
[33]G. Leising, O. Leitner, and H. Kahlert, Mol. Cryst. Liq. Cryst. **117**, 67 (1985).
[34]H. Kahlert, O. Leitner, and G. Leising, Synth. Met. **17**, 467 (1987).
[35]B. Horovitz, Phys. Rev. B **12**, 3174 (1975); D. Baeriswyl and K. Maki, Phys. Rev. B **28**, 2068 (1983).
[36]D. Emin, in *Handbook of Conducting Polymers,* edited by T. A. Skotheim (Dekker, New York, 1986), Vol. 2, p. 915, and references cited therein.
[37]D. Baeriswyl and K. Maki, Synth. Met. **28**, D507 (1989).
[38]Yu. N. Gartstein and A. A. Zakhidov, Solid State Commun. **62**, 213 (1987); **65**, ii(E) (1987).
[39]K. Maki, Synth. Met. **9**, 185 (1984).
[40]J. C. Hicks and Y. R. Lin-Liu, Phys. Rev. B **30**, 6184 (1984).
[41]J. W. Mintmire and C. T. White, Phys. Rev. B **35**, 4180 (1987).
[42]J. Ashkenazi, W. E. Pickett, B. M. Klein, H. Krakauer, and C. S. Wang, Synth. Met. **21**, 301 (1987).
[43]J. W. Mintmire and C. T. White, Phys. Rev. Lett. **50**, 101 (1983).
[44]J. W. Mintmire and C. T. White, Phys. Rev. B **28**, 3283 (1983).
[45]J. W. Mintmire and C. T. White, Bull. Am. Phys. Soc. **32**, 929 (1987).
[46]P. Vogl, D. K. Campbell, and O. Sankey, Synth. Met. **28**, D513 (1989).
[47]P. Vogl and D. K. Campbell, Phys. Rev. Lett. **62**, 2012 (1989).
[48]W. J. Feast, in *Handbook of Conducting Polymers,* edited by T. Skotheim (Dekker, New York, 1986), Vol. 1, p. 2.
[49]H. Shirakawa, T. Ito, and S. Ikeda, Macromol. Chem. **179**, 1565 (1978).
[50]M. Ozaki, D. L. Peebles, B. R. Weinberger, A. J. Heeger, and A. G. MacDiarmid J. Appl. Phys. **51**, 4252 (1980).
[51]B. Ankele, G. Leising, and H. Kahlert, Solid State Commun. **62**, 245 (1987).
[52]M. Springborg, Phys. Rev. B **33**, 8475 (1986).
[53]G. Leising, R. Uitz, B. Ankele, W. Ottinger, and F. Stelzer, Mol. Cryst. Liq. Cryst. **117**, 327 (1985); W. Ottinger, G. Leising, and H. Kahlert, in *Electronic Properties of Polymers and Related Compounds,* Vol. 63 of *Springer Series in Solid State Sciences,* edited by H. Kuzmány, M. Mehring, and S. Roth, (Springer, Heidelberg, 1986), p. 63.
[54]G. F. Koster and J. C. Slater, Phys. Rev. **95**, 1167 (1954); **96**, 1208 (1954).
[55]*Theory of the Inhomogeneous Electron Gas,* edited by S. Lundqvist and N. H. March (Plenum, New York, 1983), and references therein.
[56]D. R. Hamann, M. Schlüter, and C. Chiang, Phys. Rev. Lett. **43**, 1494 (1979).
[57]J. Ihm, A. Zunger, and M. L. Cohen, J. Phys. C **12**, 4409 (1979).
[58]O. Gunnarson and R. O. Jones, Phys. Scr. **21**, 394 (1980).
[59]The LDA or LSDA does not becomes exact in the limiting case of an hydrogen atom; the erro in the wave function is very small however, as shown by O. Gunnarsson, B. I. Lundqvist, and J. W. Wilkins, Phys. Rev. B **10**, 1319 (1974).
[60]B. Delley, P. Becker, and B. Gillon, J Chem. Phys. **80**, 4286 (1984); B. Delley, A. J. Freeman, and D. E. Ellis, Phys. Rev. Lett. **50**, 488 (1983).
[61]J. Callaway and N. H. March, in *Solid State Physics,* edited by H. Ehrenreich, F. Seitz, and D. Turnbull (Academic, New York, 1984), Vol. 38, p. 136.
[62]A discussion of recent work on structural properties with this method is given by e.g., S. Fahy and S. G. Louie, Phys. Rev. B **36**, 3373 (1987), and references therein.
[63]S. B. Trickey, F. R. Green, Jr., and F. W. Averill, Phys. Rev. B **8**, 4822 (1973).
[64]J. P. Perdew, R. G. Parr, M. Levy, and J. L. Balduz, Phys. Rev. Lett. **49**, 1691 (1982).
[65]R. W. Godby, M. Schlüter, and L. J. Sham, Phys. Rev. Lett. **56**, 2415 (1986).
[66]M. S. Hybertsen and S. G. Louie, Phys. Rev. B **34**, 5390 (1986).
[67]G. A. Baraff, M. Schlüter, Phys. Rev. B **30**, 3460 (1984).

[68]O. K. Andersen, H. L. Skriver, H. Nohl, and B. Johansson, Pure Appl. Chem. **52**, 93 (1979).
[69]A. Svane and O. Gunnarsson, Phys. Rev. B **37**, 9919 (1988).
[70]R. M. Rabe and J. D. Joannopoulos, Phys. Rev. B **36**, 3319 (1987).
[71]R. W. Jansen, R. Bertoncini, D. A. Pinnick, A. I. Katz, R. C. Hanson, O. F. Sankey, and M. O'Keeffe, Phys. Rev. B **35**, 9830 (1987).
[72]R. W. Jansen and O. F. Sankey, Phys. Rev. B **36**, 6520 (1987).
[73]G. S. Painter, Phys. Rev. B **24**, 4264 (1981).
[74]D. M. Ceperley and B. J. Alder, Phys. Rev. Lett. **45**, 566 (1980).
[75]W. Kohn and L. J. Sham, Phys. Rev. **140**, A1133 (1965).
[76]O. Gunnarsson and B. I. Lundqvist, Phys. Rev. B **13**, 4274 (1976).
[77]H. J. Monkhorst and J. D. Pack, Phys. Rev. B **13**, 5188 (1976).
[78]Y. B. Moon, M. Winokur, A. J. Heeger, J. Barker, and D. C. Bott, Macromolecules **20**, 2457 (1987).
[79]T. Tani, P. M. Grant, W. D. Gill, G. B. Street, and T. C. Clarke, Solid State Commun. **33**, 499 (1980).
[80]J. Achkenazi, W. E. Pickett, H. Krakauer, C. S. Wang, B. M. Klein, and S. R. Chubb, Phys. Rev. Lett **62**, 2016 (1989).
[81]J. E. Hirsch, Phys. Rev. Lett. **51**, 296 (1983).
[82]J. E. Hirsch and M. Grabauski, Phys. Rev. Lett. **52**, 1713 (1984).
[83]S. Mazumdar and S. N. Dixit, Phys. Rev. Lett. **51**, 292 (1983).
[84]D. K. Campbell, T. A. DeGrand, and S. Mazumdar, Phys. Rev. Lett. **52**, 1717 (1984).
[85]D. K. Campbell, T. A. DeGrand, and S. Mazumdar, Mol. Cryst. Liq. Cryst. **118**, 410 (1985).
[86]S. Kivelson, W.-P. Su, J. R. Schrieffer, and A. J. Heeger, Phys. Rev. Lett. **58**, 1899 (1987).
[87]D. Moses, A. Feldblum, E. Ehrenfreund, A. J. Heeger, T. C. Chung, and A. G. MacDiarmid, Phys. Rev. B **26**, 3361 (1982).
[88]J. Fink and G. Leising, Phys. Rev. B **34**, 5320 (1986).
[89]C. R. Fincher, M. Ozaki, M. Tanaka, D. Peebles, L. Lauchlan, A. J. Heeger, and A. G. MacDiarmid, Phys. Rev. B **20**, 1589 (1979).
[90]P. D. Townsend and R. H. Friend, Synth. Met. **17**, 361 (1987), and references therein.
[91]B. R. Weinberger, C. B. Roxlo, S. Etemad, G. L. Baker, and J. Orenstein, Phys. Rev. Lett. **53**, 86 (1984).
[92]H. Eckhardt and R. R. Chance, J. Chem. Phys. **79**, 5698 (1983); H. Eckhardt, *ibid.* **79**, 2085 (1983).
[93]G. Leising, Phys. Rev. B **38**, 10 313 (1988).
[94]R. Zemach, J. Ashkenazi, and E. Ehrenfreund, Phys. Rev. B **39**, 1884 (1989).
[95]R. Zemach, J. Ashkenazi, and E. Ehrenfreund, Phys. Rev. B **39**, 1891 (1989).
[96]W. A. Harrison, *Electronic Structure and the Properties of Solids* (Freeman, San Francisco, 1980).
[97]J. A. Majewski and P. Vogl, Phys. Rev. B **35**, 9666 (1987).
[98]O. Gunnarsson and K. Schönhammer, Phys. Rev. Lett. **56**, 1968 (1986), and references therein.
[99]D. Baeriswyl, in *Theoretical Aspects of Band Structures and Electronic Properties of Pseudo-One Dimensional Solids,* edited by H. Kamimura (Reidel, Dordrecht, 1985), p. 1.
[100]G. Lehmann and M. Taut, Phys. Status Solidi B **54**, 469 (1972).
[101]P. Vogl, in Festkörperprobleme (Advances in Solid State Physics), edited by P. Grosse (Pergamon/Vieweg, Braunschweig, 1981), Vol. 21, p. 191.
[102]D. K. Campbell and A. R. Bishop, Phys. Rev. B **24**, 4859 (1981).
[103]R. Chance, D. S. Boudreaux, J. L. Brédas, and R. Silbey, in *Handbook of Conducting Polymers,* edited by T. A. Skotheim (Dekker, New York, 1986), Vol. 2, p. 825.
[104]W. P. Su, in *Handbook of Conducting Polymers,* edited by T. A. Skotheim (Dekker, New York, 1986), Vol. 2, p. 757.
[105]S. Phillpot, D. Baeriswyl, A. R. Bishop, and P. Lomdahl, Phys. Rev. B **35**, 7533 (1987).
[106]A. R. Bishop, D. K. Campbell, P. S. Lomdahl, B. Horovitz, and S. R. Phillpot, Phys. Rev. Lett. **52**, 671 (1984).
[107]R. Ball, W. P. Su, and J. R. Schrieffer, J. Phys. (Paris) Colloq. **44**, C3-429 (1982).
[108]M. T. Yin and M. L. Cohen, Phys. Rev. B **26**, 3259 (1982).
[109]M. A. Majewski and P. Vogl, in *Electronic Properties of High-T_c Superconductors and Related Compounds,* Vol. X of *Springer Series in Solid-State Sciences,* edited by H. Kuzmány, M. Mehring, and J. Fink (Springer, Heidelberg, in press).
[110]T. Ito, H. Shirakawa, and S. Ikeda, J. Polym. Sci. Polym. Ed. **12**, 11 (1974).
[111]G. Leising, H. Kahlert, and O. Leitner, in *Electronic Properties of Polymers and Related Compounds,* Vol. 63 of *Springer Series in Solid-State Sciences,* edited by H. Kuzmány, M. Mehring, and S. Roth (Springer, Heidelberg, 1986), p. 56.
[112]H.Thomann and G. L. Baker, J. Am. Chem. Soc. **109**, 1569 (1987).
[113]D. Baeriswyl, Helv. Phys. Acta **56**, 639 (1983).
[114]L. Rothberg, T. M. Jedju, S. Etemad, and G. L. Barker, Phys. Rev. B **36**, 7529 (1987).
[115]S. T. Pantelides, Phys. Rev. B **36**, 3479 (1987); M. K. Sheinkman, in *Proceedings of the 18th International Conference on the Physics of Semiconductors,* edited by O. Engström (World Scientific, Singapore, 1987), p. 785.
[116]D. Baeriswyl, J. Phys. (Paris) Colloq. **44**, C3-381 (1983).
[117]G. W. Bryant and A. J. Glick, Phys. Rev. B **26**, 5855 (1982).
[118]H. Bleier, K. Donovan, R. H. Friend, S. Roth, L. Rothberg, R. Tubino, Z. Vardeny, and G. Wilson, Synth. Met. **28**, D189 (1989).

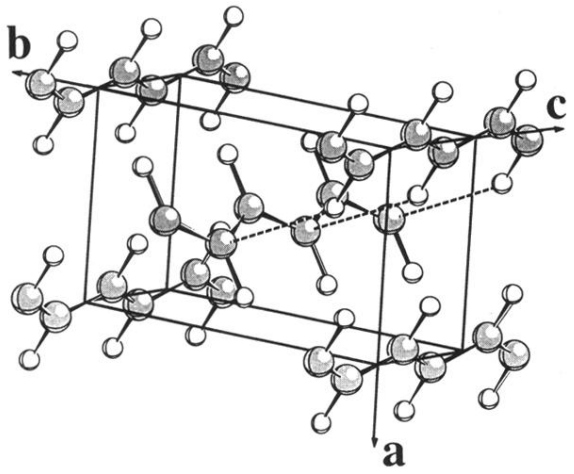

FIG. 2. Conventional unit cell of *trans*-$(CH)_x$ in the $P2_1/a$ structure. The dashed lines are drawn to emphasize a characteristic feature of this structure: the hydrogen atoms of one chain point approximately towards the carbon atoms of the neighboring chains.

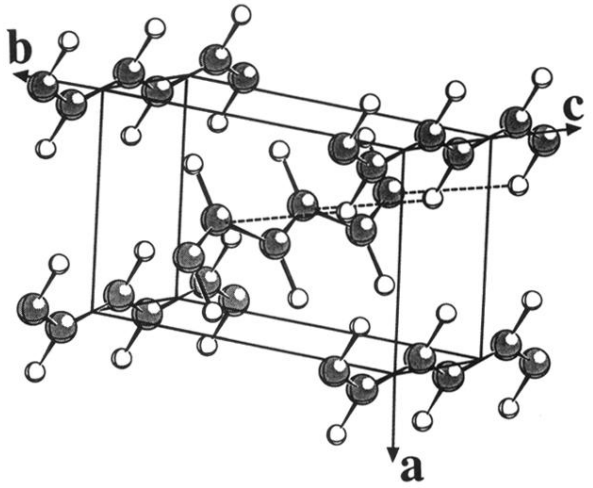

FIG. 3. Conventional unit cell of *trans*-$(CH)_x$ in the $P2_1/n$ structure. As in Fig. 2, the dashed lines emphasize the approximate alignment of the carbon and hydrogen atoms on adjacent chains. However, these atoms are further apart in the $P2_1/n$ structure than in the $P2_1/a$ structure.

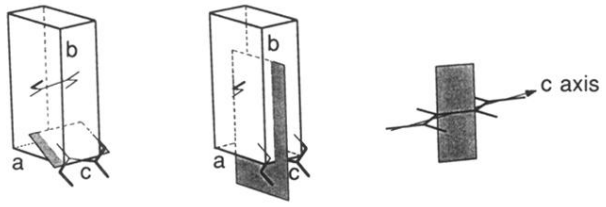

(a) (b) (c)

FIG. 5. The computed electronic charge density surfaces in the following figures refer to one of the plane sections of the unit cell shown here: (a) the plane of the carbon-hydrogen σ bonds. (b) The plane perpendicular to that shown in (a) and parallel to the carbon-hydrogen bond in one chain. This plane section displays the carbon π bonds and also illustrates the charge distribution between the chains. (c) The plane perpendicular to that shown in (a) and parallel to the carbon-carbon bond.